CHARACTERIZATION OF ION IMPLANTED SURFACES BY LASER INDUCED BREAKDOWN SPECTROSCOPY, LIBS

A Thesis Submitted to
the Graduate School of Engineering and Science of
İzmir Institute of Technology
in Partial Fulfillment of the Requirements for the Degree of

MASTER OF SCIENCE

in Chemistry

by
Sabiha ÖRER

January 2008

İZMİR

We approve the thesis of **Sabiha ÖRER**

Assoc. Prof. Dr. Şerife YALÇIN
Supervisor

Prof. Dr. Orhan ÖZTÜRK
Committee Member

Asst. Prof.Dr. Ritchie EANES
Committee Member

2 January 2008
Date

Prof. Dr. Levent ARTOK
Head of Department of Chemistry Department

Prof. Dr. Hasan BÖKE
Dean of the Graduate School of Engineering and Science

ACKNOWLEDGMENT

I have been accompanied and supported by many people during this thesis study. I have now the opportunity to express my gratitude to all of them.

The first person I would like to thank is Assoc. Prof. Dr. Şerife YALÇIN who not only guided me as my supervisor but also encouraged, and challenged me throughout my master program. Her wide knowledge and her logical way of thinking have been of great value to me.

My sincere thanks to Prof. Dr. Raşit TURAN for his generosity of letting us use their Ge implanted samples.

Prof. Dr. Orhan ÖZTÜRK, Asst. Prof. Dr. Ritchie EANES, Prof. Dr. Serdar ÖZÇELİK and Asst. Prof. Dr. Süleyman TARI deserve a special thanks as my thesis committee members. I would like to thank all of them for their valuable comments and suggestions.

Moreover, I am grateful to Asst. Prof. Dr. Çağlar KARAKAYA for sharing his optical microscope and Assoc. Prof. Dr. Salih OKUR for AFM measurements.

My appreciation and thanks for the accomplishment of this study are directed to group members of the Materials Research Center of İYTE for the SEM-EDX and AFM analyses.

I am pleased to acknowledge TUBITAK for financial support (Project No. 105T134) .

I also feel deeply indebted to my research friend Resch. Assist. Arzu ERDEM not only because of her friendship but also for her kind efforts and endless support.

I would like to thank all my friends at İYTE, especially Resch. Assist. Pınar KASAPLA and Burcu ALTIN for their unfailing encouragement, neverending friendship and support during my thesis.

Lastly, and most importantly, I wish to thank my family. I especially thank to Evren MERT for making a difference in my life, to my parents Hikmet and Hüseyin ÖRER and to my sister Gülümser ÖRER for their love and support all through my life. With my deepest gratitude, I dedicate this study to my family.

ABSTRACT

CHARACTERIZATION OF ION IMPLANTED SURFACES BY LASER INDUCED BREAKDOWN SPECTROSCOPY, LIBS

Laser Induced Breakdown Spectroscopy, LIBS, is a versatile atomic emission spectrometric technique for the determination of the elemental composition of solids, liquids, gases and aerosols with the need for little or no sample preparation.

In this study, an optical LIBS system from its conventional parts was designed, constructed and optimized for spectrochemical analysis of solid materials. Specifically, the 2-D elemental distribution of Ge ions on silicon oxide surfaces, prepared by the method of ion implantation, with differing atomic concentrations between 10^{16} - 10^{17} ions/cm^2 have been investigated by LIBS. For this purpose a Nd: YAG laser operating at the second harmonic wavelength, 532 nm, was used to create a plasma on the material surfaces. Spatially and temporally resolved atomic emission from the luminous plasma was detected by an Echelle spectroctrograph and Intensified Charged Coupled Device (ICCD) detector combination.

Spectral emission intensity from the LIBS measurements has been optimized with respect to time, crater size, ablation depth and laser energy. Atomic Force Microscopy (AFM) and Scanning Electron Microscopy (SEM) coupled with Energy Dispersive X-Ray Spectroscopy (EDX) have been utilized to obtain crater depth, morphology and elemental composition of the sample material, respectively. LIBS spectral data revealed the possibility of performing 2-D distribution analysis of Ge ions over the silicon oxide substrate at Ge ion concentrations lower than 0.5% (atomic). LIBS as a fast semi-quantitative analysis method with 50µm lateral and 800 nm depth resolutions has been evaluated. In this wok, elemental analysis of some metal surfaces, such as Al and Cu, was also performed by LIBS.

Keywords: LIBS, surface analysis, Ge ion implantation, lateral resolution,

ÖZET

LAZER OLUŞTURMALI PLAZMA SPEKTROSKOPİSİ, LIPS, İLE İYON EKİLMİŞ YÜZEYLERİN KARAKTERİZASYONU

Lazer Oluşturmalı Plazma Spektroskopisi, LIBS, malzeme hazırlama işlemi en az seviyede ya da hiç olmadan, katı, sıvı, gaz ve aerosollerin elemental kompozisyonunu belirlemede son yıllarda yaygın olarak kullanılan bir atomik emisyon spektrometresi tekniğidir.

Bu çalışmada, katı malzemelerin spektrokimyasal analizleri için bir Lazer Oluşturmalı Plazma Spektrometresinin tasarım, kurulum ve optimizasyon çalışmaları gerçekleştirilmiştir. Özellikle, 10^{16} - 10^{17} iyon/cm^2 iyon konsantrasyonlarında iyon ekleme metodu ile silikon oksit yözeyine ekilmiş germanyum iyonlarının 2-boyutlu elemental dağılımı incelenmiştir. Bu amaçla, bir Nd: YAG lazerinin 532 nm'deki ikincil harmonik ışıması kullanılmıştır. Oluşan ışıklı plazmanın atomik emisyonu, Eşel tipi bir spektrograf ve şiddetlendirilmiş bir CCD detektör, ICCD, ile uzamsal ve zamansal olarak incelenmiştir.

Laser Oluşturmalı Plazma ölçümlerinden elde edilen spektral emisyon şiddeti, zaman, krater büyüklüğü, aşındırma derinliği ve lazer enerjisi bakımından optimize edilmiştir. Oluşan kraterlerin derinliğini, morfolojisini ve elemental kompozisyonunu belirlemede Atomik Kuvvet Mikroskobu (AFM) ve Enerji Dağılımlı X-Ray spektroskopisi ile eşleştirilmiş Taramalı Elektron Mikroskobu (SEM), kullanılmıştır. LIBS spektral verileri, silikon oksit üzerine ekilmiş Ge iyonlarının iki boyutlu (2-D) elemental kompozisyon dağılımının % 0,5 (atomik) den daha az miktarlarda tayin edilebileceğini göstermiştir. Kurulan LIBS sisteminin 50µm yüzeysel ve 800 nm derinlik çözünürlüğünde hızlı bir yarı-kantitatif analiz metodu olarak kulanılabilirliği değerlendirilimiştir. Ayrıca Al ve Cu gibi metal yüzeylerinin elemental analizleri de yapılmıştır.

Anahtar kelimeler: LIPS, yüzey analizi, Ge iyonu ekimi, yanlamasına çözünürlük.

TABLE OF CONTENTS

LIST OF FIGURES viii
LIST OF TABLES ix

CHAPTER 1. INTRODUCTION 1
1.1. Laser Induced Breakdown Spectroscopy, LIBS 1
1.2. Advantages and Disadvantages of Laser Induced ..... Breakdown Spectroscopy, LIBS 2
1.3. Laser Induced Breakdown Spectroscopy Instrumentation 3
1.3.1. Lasers 3
1.3.1.1. Solid-State Lasers 5
1.3.1.2. Gas Lasers 5
1.3.1.3. Dye Lasers 6
1.3.1.4. Semiconductor Diode Lasers 6
1.3.2. Focusing and Collection Optics 6
1.3.3. Spectrograph & Detector 6

CHAPTER 2. SURFACE ANALYSIS BY LIBS 9
2.1. Surface Analysis 9
2.1.1. Two Dimensional (2-D) Compositional Mapping 9
2.1.2. Depth Profiling 10
2.2. Aim of Study 12
2.3. Applied Methods 12
2.3.1. Scanning Electron Microscopy (SEM) 13
2.3.2. Atomic Force Microscope (AFM) 14

CHAPTER 3. EXPERIMENTAL 15
3.1. Materials 15
3.1.1. Silicon 15
3.1.2. Germanium 15
3.1.3. Ion Implantation 16
3.2. LIBS Experimental Set-up 17

3.3. SEM/EDX Analysis 19
3.4. AFM Analysis 20

CHAPTER 4. RESULTS AND DISCUSSION 21
4.1. Spectral Analysis by LIBS 21
4.2. Signal Optimization 27
4.2.1. Focusing Lens to Sample Distance Adjustment 27
4.2.2. Time Resolution 28
4.2.3. Germanium Signal Intensity and Implantation Dose 30
4.2.4. Effect of Laser Energy 31
4.2.5. Crater Size 33
4.3. Two Dimensional (2-D) Compositional Mapping 35
4.3.1. LIBS Analysis 35
4.3.2. SEM/EDX Analysis 39
4.4. Depth Analysis 42
4.4.1. AFM Analysis 42
4.4.2. LIBS Spectral Analysis 44

CHAPTER 5. CONCLUSIONS 45
REFERENCES 46

LIST OF FIGURES

Figure **Page**

Figure 1.1. A typical LIBS set up. 3
Figure 1.2. A laser and its components........ 4
Figure 1.3. An echelle polychromator system. 7
Figure 1.4. ICCD detector........ 8
Figure 3.1. Schematical representation of ion implantation process 16
Figure 3.2. Experimental setup for LIBS........ 18
Figure 4.1. Typical LIBS emission spectrum of an Al target. 23
Figure 4.2. Typical LIBS emission spectrum of a Cu target 24
Figure 4.3. Typical LIBS emission spectrum of a pure silicon wafer. 25
Figure 4.4. Typical LIBS emission spectrum of Ge implanted silicon wafer. 26
Figure 4.5. Optical microscope images for focusing lens........ 27
Figure 4.6. Time resolved spectra of Ge implanted samples at several
gate delay times and laser pulses 29
Figure 4.7. Germanium growth curves for Ge (303.9 nm) line 30
Figure 4.8. Relative signal intensities at different laser energies. 32
Figure 4.9. SEM images of the craters........ 34
Figure 4.10. Relationship of laser energy to crater size........ 35
Figure 4.11. SEM image of the Ge-ion implanted Si wafer 36
Figure 4.12. Ge ion distribution on implanted SiO_2 surfaces. 38
Figure 4.13. Contour plot showing the 2-D Ge ion distribution on
as SiO_2 matrix. 39
Figure 4.14. SEM image of a 33.88 μm crater 40
Figure 4.15. SEM-EDX line scans analysis for Ge ion distribution........ 42
Figure 4.16. Atomic force microscope image........ 43
Figure 4.17. Relative intensities of Si-288.15 and Ge-303.91 nm lines........ 44

LIST OF TABLES

Table **Page**

Table 3.1. LIBS system specifications 19
Table 4.1. Spectral emission wavelengths of materials used. 21
Table 4.2. SEM-EDX measurements 41

CHAPTER 1

INTRODUCTION

1.1. Laser Induced Breakdown Spectroscopy, LIBS

Lasers have been proposed and utilized as atomization sources in analytical atomic spectroscopy, for decades. **L**aser **I**nduced **B**reakdown **S**pectroscopy, LIBS, is a spectrochemical analysis technique in which lasers are used for vaporization, atomization and ionization steps. LIBS is also known as Laser Induced Plasma Spectroscopy (LIPS) and Laser Ablation Spectroscopy (LAS).

In LIBS, a powerful laser pulse is brought to a sharp focus onto a target (solid, liquid, or gas) by using a focusing lens. A thin layer of the material is spontaneously ablated from the target surface, and then it subsequently gains energy from the laser beam. The ablated material is suddenly heated by generating hot plasma with a temperature of nearly 20,000 K and an electron density of 10^{16} – 10^{20} electrons/cm^3 (Sneddon 1997). At these temperatures, the ablated material breaks down into excited ionic and atomic species. The spectral emission of these species is collected by suitable optical lenses and sent onto the entrance slit of a spectrograph and a detector. Spectral analysis of the plasma can be used to determine the elemental composition, spatial distribution and several other properties of ablated sample (Sneddon 1997).

LIBS has been used in a variety of applications including : the Mars exploration (Brennetot 2003, Cremers 2000), cultural heritage studies (Anglos 2007), identification of bioaerosols (Dixon, et al. 2005), trace element analysis of powdered samples (Gondal 2006), enviromental monitoring of heavy metals (Mirov 1999), identification of teeth affected by caries (Samek 2001), and analysis of papers (Häkänken 2001).

1.2. Advantages and Disadvantages of Laser Induced Breakdown Spectroscopy, LIBS

Laser Induced Breakdown Spectroscopy, LIBS has been evaluated as an alternative method to other conventional plasma atomic emission spectrometric techniques, such as, Inductively Coupled Plasma Atomic Emission Spectrometry, (ICP-AES), and Direct Current Plasma Atomic Emission Spectrometry, (DCP-AES), Microwave Induced Plasma (MIP-AES), Arc-AES, Spark-AES, Glow Discharge-OES or even Glow Discharge-Mass Spectrometry (Winefordner 2004).

Several significant advantages make LIBS more applicable than others as follows:

i) Little or no sample preparation makes it quick and easily adaptable to chemical monitoring equipments or portable units;

ii) LIBS is capable of determining elemental compositions of various materials regardless of whether the sample is solid, liquid, gas or aerosol;

iii) Since it is an emission technique, direct analysis of plasma provides simultaneous multi-elemental analysis;

iv) The technique can be used to analyze extremely hard materials that are difficult to digest and dissolve;

v) The spatial and temporal resolution is high since plasma light is extremely bright, so that all atomic species are accessible; and

vi) There is also the option of using LIBS for remote analyses. (Winefordner 2004).

However, difficulty in obtaining suitable standards is a disadvantage for LIBS. Thus, LIBS can be considered a semiquantitative analysis technique. LIBS has poor precision typically ranging between 5-10 % mainly due to the fluctuations in laser energy and shot-to-shot reproducibility (Winefordner 2004).

1.3. Laser Induced Breakdown Spectroscopy Instrumentation

A typical LIBS system consists of a pulsed laser, a focusing lens, collection lenses and a spectrometer with a wide spectral range and a high sensitivity, fast response rate, time-gated detector (Figure 1.1).

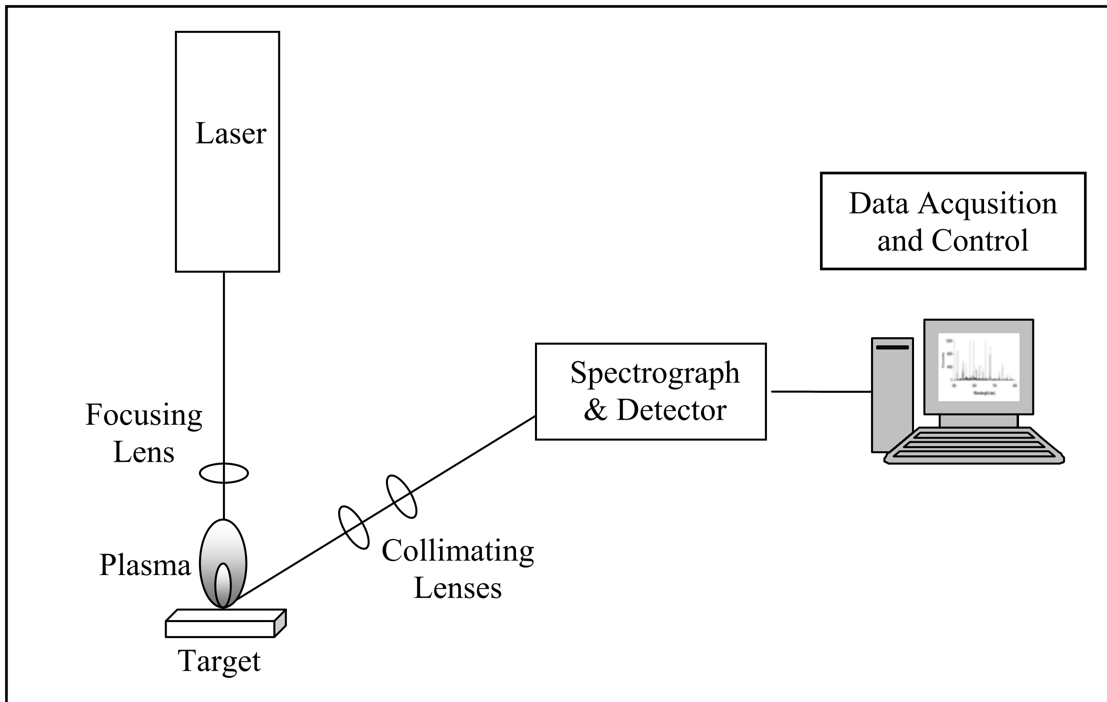

Figure 1.1. A typical LIBS set up
(Source: Radziemski 1989)

In this section each part of the typical LIBS system components will be explained in detail.

1.3.1. Lasers

The word **LASER** is an acronym for **L**ight **A**mplification by **S**timulated **E**mission of **R**adiation. A laser is a quantum-mechanical device that creates and amplifies a narrow, intense beam of coherent light. A laser consists of an active lasing medium, a high reflective mirror and a partially transmissive mirror (output coupler) (Figure 1.2).

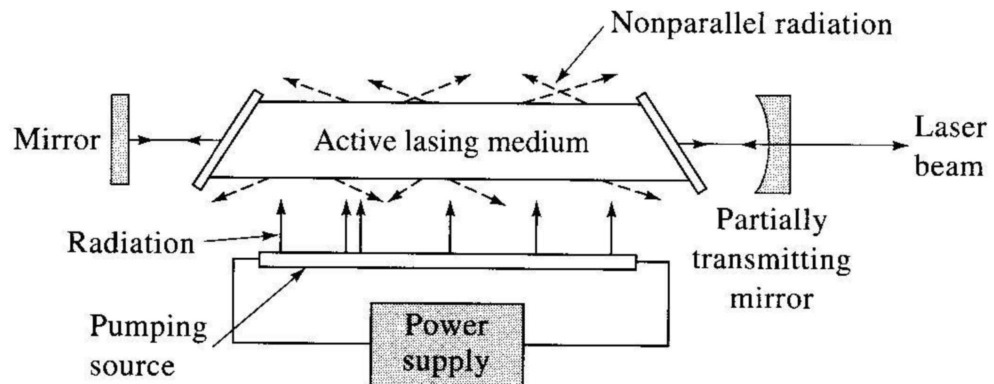

Figure 1.2. A laser and its components
(Source: Skoog, et al. 1997)

The active lasing medium is the heart of the laser and may be in the form of gas, liquid, solid or free electrons. This lasing medium is energized or pumped by an external energy source (electricity or flash lamps) and absorbs this energy. Consequently, electrons in the active medium are excited to higher energy levels. Population inversion is successful if the number of particles in one excited state exceeds the number of particles in some lower-energy state. Thus, stimulated emission is observed and light is amplified (Skoog, et al. 1997).

An optical cavity consists of a pair of mirrors arranged such that light is reflected back and forth by passing through the active medium. Throughout each passage, the intensity of light is amplified by generation of additional photons. One of the mirrors in the optical cavity is partially transparent and is called the output coupler. The output laser beam is emitted through this mirror (Skoog, et al. 1997).

Lasers are generally classified according to laser material and pump material. Silfvast et al. (1996) notes that the major types of lasers are as follows:

- Solid state lasers
- Gas lasers
- Dye lasers
- Semiconductor diode lasers.

1.3.1.1. Solid-State Lasers

Solid-state lasers (Siegman 1986) use solids as an active lasing medium and are optically pumped with discharge lamps or laser diodes. Generally, the active medium of these types of lasers consist of a crystal or glass doped with a small amount of rare earth elements or transition metal ions such as neodymium, chromium or erbium (Sneddon 1997). In solid-state lasers, a high or low output power (a few milliwatts or many kilowatts) with a high beam quality and ultra short pulses with nanosecond, picosecond or femtosecond durations can be achieved. There are many hundreds of solid-state media in which laser action has been achieved, but relatively few types are in widely used. Nd:YAG, Er:Yb:glass, Nd:YLF, Cr:YAG, Ti:sapphire and ruby are examples of common solid-state lasers (Silfvast, et al. 1996).

The Nd:YAG laser is the most common type of solid-state laser and widely used in LIBS as a plasma source. A neodymium (Nd^{+3}) ion is doped into a crystal of yttrium aluminum garnet ($Y_3Al_5O_{12}$). The Nd:YAG laser generates energy in the near infrared region of the electromagnetic spectrum, with wavelength of 1064 nm (Skoog, et al. 1997). Other emission wavelengths can be obtained by frequency doubling (532 nm) (Sauter 1996), frequency tripling (355 nm) and frequency quadrupling (266 nm).

Femtosecond lasers are also a class of solid-state lasers in which pulse durations can range from a few femtoseconds to several hundreds of femtoseconds. A femtosecond laser emits optical pulses with a duration well below one picosecond, in the domain of femtoseconds. Femtosecond lasers have several advantages for applications, such as micromachining, (Bärsch 2003), due to smooth and clean craters formed as a result of decreased laser-matter interaction.

1.3.1.2. Gas Lasers

Gas lasers (Siegman 1986) use a gas or a mixture of gases as an active medium and are pumped with electrical discharges. There are many different types of gas lasers such as He-Ne lasers, nobel gas ion lasers (i.e. Ar-ion lasers), CO_2 lasers, N_2 lasers, and excimer lasers (rare gas halide lasers). The most common and inexpensive gas laser is the He-Ne laser and is usually operated in the red region near 632.8 nm. Except for the

He-Ne laser, all other types of pulsed gas lasers can be used in LIBS for plasma production.

1.3.1.3. Dye Lasers

Dye lasers (Siegman 1986) are based on the use of a dye as the active medium, which can be tuned from the ultraviolet to near infrared. Most dye lasers are fluorescent organic molecules dissolved in a liquid solvent.

1.3.1.4. Semiconductor Diode Lasers

Semiconductor diode lasers (laser diodes) (Siegman 1986) use semiconductor materials as the active medium and can be electrically pumped. The most common semiconductors used in laser diodes are gallium arsenide, indium gallium arsenide phosphide and gallium nitride.

1.3.2. Focusing and Collection Optics

Focusing optics bring the parallel beam from the laser to a focused spot. Since the size of the spot and depth of focus depends on the focusing optics, choosing the right lens type is important.

The collimating optics are used to bring the plasma light to a parallel beam and then bring it again to a focused spot. Thus, the plasma light is focused onto the entrance slit of the detector (Silfvast 1996) with the use of a pair of lenses.

1.3.3. Spectrograph & Detector

Regardless of the sample type being analyzed, the plasma light is analyzed in the same way. Typically, emission from the atoms and ions in the plasma is collected by a lens or fiber optics and sent to a spectrograph and a detector. LIBS is usually composed of either a monchromator (i.e. Czerny-Turner type) or a polychromator (Echelle type) and a photomultiplier tube or an intensified charged coupled device detector (CCD) combination (Sneddon 1997).

The use of Echelle type polychromators is ever increasing whilst Czerny-Turner is the most widely used monochromator type (Sneddon 1997). A system based on an echelle spectrograph offers a combination of high resolution and wide wavelength range

by using a grating with a large groove spacing. In an echelle spectrograph, there are two dispersing elements: a) an echelle grating, or a diffraction grating and b) a low-dispersion grating, or a prism (Figure 1.3). A diffraction grating has widely spaced grooves. The light is diffracted in a standard grating at normal incidence to the face of grooves. Therefore, a series of overlapping spectra with high resolution are produced. A low dispersion grating, or a prism, placed perpendicular to the echelle is used for separating out the overlapping spectra (Skoog, et al. 1997).

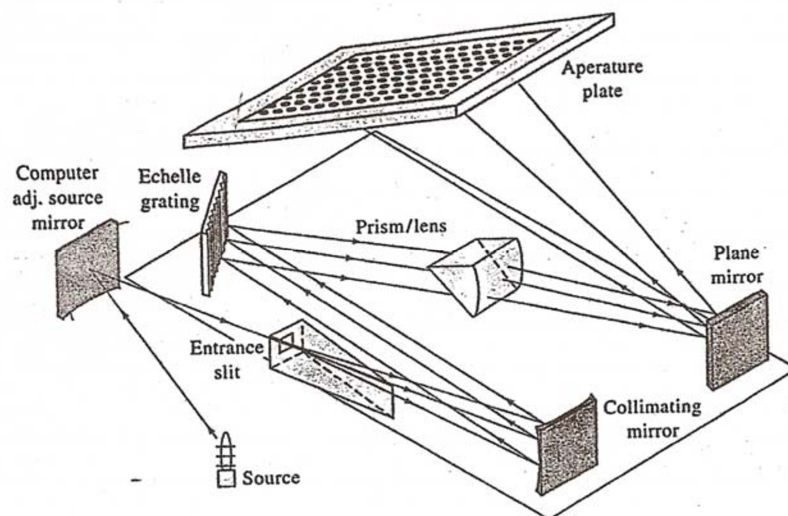

Figure 1.3. An echelle polychromator system
(Source: Skoog, et al. 1997)

The grating is used over a smaller range of angles so that it can be blazed with a well-shaped groove to be more efficient in a very wide range of wavelengths. This is the main advantage of an echelle spectrograph (Skoog, et al. 1997).

The plasma light is imaged on the entrance slit of a scanning monochromator or a spectrograph to be resolved spectrally with a photomultiplier tube (PMT), photodiode array (PDA) or intensified charged coupled device (ICCD) (Sneddon 1997).

A charged coupled device (CCD) with an image intensifier tube is called intensified charged coupled device (ICCD) and is usually attached to a spectrograph

(Figure 1.4) An image intensifier tube is an electronic tube consisting of a photocathode, micro-channel plate (MCP) and an anode (phosphor screen). In an image intensifier tube: the photons arrive at the photocathode that is located in the image (focal) plane of the tube.

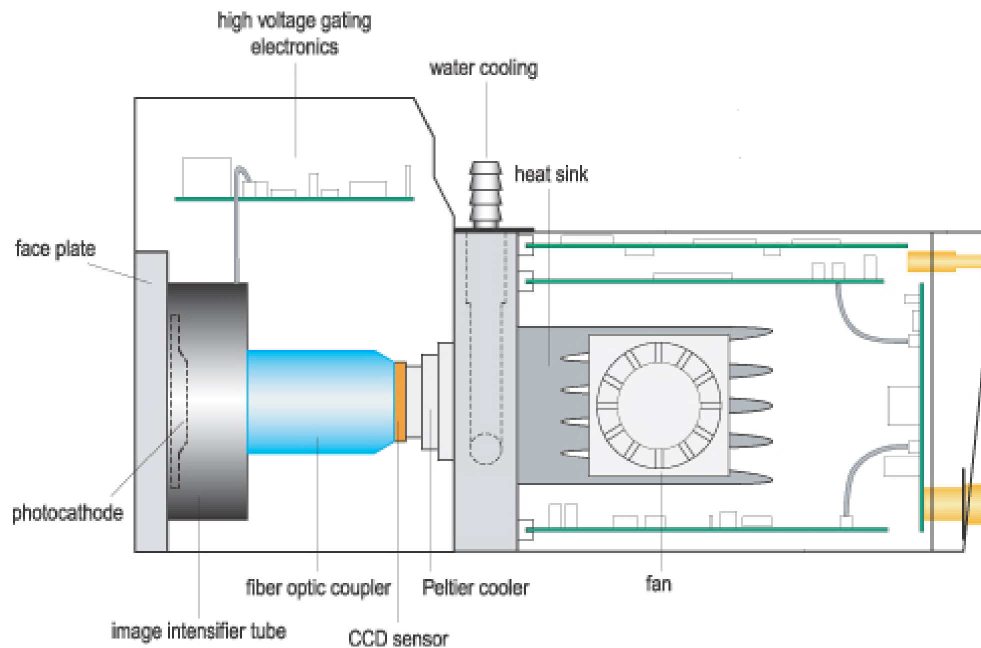

Figure 1.4. ICCD detector
(Source: Andor Technology 2007)

At the cathode, the photons are converted into electrons that are than sent into the vacuum of the image intensifier. The electrons are accelerated to the MCP because of the negative charge of the photocathode. The MCP is a multichannel plate: each channel multiplies the number of incoming electrons. The out-coming electrons are accelerated towards the anode, which is a phosphor screen in which the electron energy is converted into photons. The image is thus intensified and then transferred to the CCD of the camera either by a fiber optic coupling or by a lens coupling. The main advantage of an ICCD camera is to image acquisition at very low light levels at relatively high speed (Andor Technology 2007).

CHAPTER 2

SURFACE ANALYSIS BY LIBS

2.1. Surface Analysis

Laser induced breakdown spectroscopy (LIBS) can be applied to many different types of samples. However, most applications of LIBS are based on analysis of solid materials (Winefordner, et al. 2004).

Recent studies (Taschuk, et al. 2005, Cravetchi, et al. 2004) have focused on the ability of LIBS for surface analysis by 2-D compositional mapping and depth profiling analysis. Multielemental distribution analysis of sample surfaces is achieved by scanning different points of the surface with a tightly focused laser beam while successive laser pulses on the same point provide information on depth profiling. Depending on the repetition rate of the laser applied, these analyses can be obtained quickly and easily (Laserna 2004) compared to other types of surface analysis techniques.

2.1.1. Two Dimensional (2-D) Compositional Mapping

LIBS has been used for two dimensional compositional mapping by several researchers. There are many studies that have been performed by LIBS in order to identify impurities in Al alloys, or investigate the spatial resolution of LIBS on steel samples. Bette and Noll (2003) evaluated LIBS for scanning microanalysis up to 1kHz repetition rate. A diode pumped Q-switched Nd: YAG laser was focused on steel samples. Intervals of 20 μm were choosen due to the size of crater (15 μm) obtained by a single laser pulse with 2 μJ energy and 1x1 cm^2 of surface were scanned. They showed that a lateral resolution of 20 μm could be achieved with a LIBS system. Also they showed that LIBS as a fast technique for analysis of elemental distributions when compared with SEM-EDX.

Spectrochemical microanalysis of aluminum alloys was performed using a Ti-Sapphire laser system with 130 fs pulse duration at 800 nm by Cravetchi et al. (2006).

Multielemtal microanalysis of commercial Al alloys was carried out with a lateral resolution of 10 μm at a pulse energy of 7 μJ. It was also stated that precision and spatial resolution can be improved by using single UV femtosecond laser pulses which results in higher and more reproducible absorption.

Rieger et al. (2002) showed the capability of LIBS for microanalysis at low energies with high spatial resolution. Aluminum alloys were analyzed with a KrF excimer laser operating at 298 nm at laser pulse energies in the range of 100 to 300 μJ. Spatial resolution was achieved in the range of 15 to 30 μm which is the diameter of the ablation craters.

2.1.2. Depth Profiling

Investigation of spatially resolved structures has started an interest in modern analytical methods for depth profile analysis in the μm to nm range. Depth profiling is the compositional knowledge of interface between different layers. Laser Induced Breakdown Spectroscopy (LIBS) can be used as a surface and depth analysis method capable of performing direct, fast and easy analysis at atmospheric pressure with comparable resolution of any sample regardless its nature, size and shape.

A typical pulsed laser forms craters on the target surface varying in depth from nanometers to micrometers. Sequential laser pulses on the same spot provides information on the atomic composition of the material as a function of depth (Laserna 1998, Laserna 2001). Several techniques are used to determine atomic depth profiling. The most widely used are, Auger Electron Spectroscopy (AES), X-Ray Photoelectron spectroscopy (XPS), Secondary Ion Mass Spectroscopy (SIMS) and Glow-Discharge spectroscopy (GD). However, these techniques have some limitations; neither XPS nor SIMS can be directly applied to the depth profiling of thicker (micrometer) layers and cannot be applied to any fast on-line processes (Laserna 2001). Nowadays, glow-discharge optical emission and mass spectrometry (GD-OES and GD-MS) are the most widespread techniques used due to their excellent depth resolved capabilities, short-term stabilization time, the reduction of matrix effects, good reproducibility and accuracy. However, the poor lateral precision (at best a few mm), limitations of sample shape and dimensions for the sample chamber, necessity of low-pressure conditions and Ar interference are the restrictions for GD (Laserna 2001, Hergenröder 2001). LIBS has

been used as an alternative method for depth profiling. There are several studies performed by LIBS.

Laserna et al. (1997) analyzed electrically deposited commercial brass samples, which contain a Zn-Cu alloy and different elements with minor percentages. A pulsed Nd: YAG laser (80 mj/pulse, 5 ns pulse duration) at the second harmonic level (532 nm) was used to show applicability of LIBS to depth profiling analyses. The coated samples were ablated by firing the laser repetitively on a single point. It was found that ablation rate was at the ng per pulse level and depended on laser irradiance.

Milan et al. (1998) detected depth profiling of phosphorous doping in silicon using a Nd: YAG laser at 532 nm. For these studies the plasma emission was detected with a charged coupled device (CCD). This study demonstrated the capabilities of LIBS for depth profile analysis of phosphorus doping in silicon. Depth resolution was found to be nearly 1.2 mm.

Romero and Laserna (1998) analyzed carbon impurities on a photonic grade silicon wafer with a total area of 3x2.1 mm^2, a lateral resolution of 70 µm and at a depth resolution of about 160 nm. A pulsed nitrogen laser was focused on the silicon surface to create the plasma. It was concluded that 2D and 3D characterization of surfaces can be done by LIBS with improvement of focusing optics and the use of lasers having a more homogenous energy distribution.

Laserna et al. (2000) employed several angles of incidence of the laser beam to increase resolution in depth profiling. A Cr layer deposited on a Ni foil and Sn-coated steels were treated with a XeCl excimer laser at 308 nm (28 ns pulse duration). It was shown that there is an improvement in depth resolution with increasing incidence angle. It was also reported that ablation rate was lower than 2 nm per pulse using a combination of collimated beam ablation and angle resolved measurements.

Laserna et al. (2001) also demonstrated that ablation rate and depth resolution are related to irradiance (power density, energy per pulse beam size) in depth profiling studies of LIBS. Ni-Cu-coated brass samples were examined at a fixed laser wavelength, pulse width and experiment geometry to show the effects of laser irradiance on average ablation rate and depth resolution. The laser irradiance increased by either focusing the laser beam or increasing the pulse energy. Their results showed that the best depth resolution could be achieved by keeping irradiance at moderate conditions (irradiance range: 60-111 MW cm^{-2}).

Hergenröder et al. (2001) conducted an experiment with Cu-Ag and TiN-TiAlN multilayers on silicon and iron samples. The thickness of each individual Cu-Ag and TiN-TiAlN layers were measured at 600 nm and 280 nm in Ar (in a range 10-1000 mbar). The ablation rate was changed in the range between 10-30 nm per pulse for the laser fluence of 0.5-1.51 joule per cm^{-2} from a femtosecond laser. A spatial resolution of 10 nm per pulse was obtained for the TiN-TiAlN double layers.

Bustamante et al. (2002) tested LIBS as a method for the analysis of Ca in a soil of Patagonia (Argentina). The use of LIBS for in-situ applications was stated as an advantage for determining total and insoluble Ca in soil under optimum experimental operating conditions. LIBS has been compared with other volumetric volumetric titration techniques. The results revealed that LIBS has an advantage over these volumetric techmiques with the possibility of *in-situ* applications.

Mateo et al. (2006) used LIBS to show the capability of linear correlation for depth profiling of different archeological ceramics and polymer coatings on steel. Linear correlation measures the degree of interrelation between two variables, x and y, through the linear correlation coefficient, r. Depth profiles were extracted using the software by plotting the evolution of the linear correlation coefficient values. The more useful results were obtained with the correlated LIBS analysis.

2.2. Aim of Study

In this study, the primary goal was to design, construct and optimize an optical LIBS system at İYTE from its conventionally purchased parts for elemental analysis of solid surfaces. Elemental detection of Ge atoms on implanted silicon surfaces, with ion concentrations as low as $10^{16}/cm^2$, was the second goal. Hence, some factors effecting lateral and depth resolution such as laser energy, crater size and spot size were investigated. After determining and optimizing these conditions, 2-D surface mapping of ion implanted surfaces, laterally and in depth, were performed.

2.3. Applied Methods

Two methods are commonly used in order to measure crater size and depth of craters formed by laser pulses, scanning electron microscopy (SEM) for crater size measurements and atomic force microscope (AFM) for depth measurements.

2.3.1. Scanning Electron Microscopy (SEM)

A scanning electron microscope is a type of electron microscope that uses electrons to form an image of a sample. SEM enables the surface scientist to obtain topographical and high-resolution images of a sample surface by scanning the surface with a beam of energetic electrons. The higher magnification as well as the ease of sample preparation and observation makes it useful in research areas.

In the methodology, a beam of electrons is focused on the surface of the sample. The sample surface is bombarded with an electron beam of several keV and the sample is scanned in a raster pattern. These bombarding electrons are called primary electrons. The primary electrons cause emission of electrons from the sample itself. These emitted electrons are known as secondary electrons. Secondary electrons are collected by a grid or detector and finally translated into images of the topography being analyzed. The brightness of the signal depends on the number of secondary electrons reaching the detector. The primary electrons also result in the emission of backscattered (or reflected) electrons from the sample. Backscattered electrons have more energy (50 keV) than secondary electrons, and have a definite direction (Skoog, et al. 1997).

An SEM may be equipped with an Energy Dispersive X-Ray (EDX) analysis system. EDX analysis is useful for identifying materials and contaminants, and their relative concentrations on the surface of the specimen. During EDX analysis, the bombarding electrons interact with the electrons of samples atoms. An inner shell electron is ejected. Then its position is filled with a higher energy electron from an outer shell by emitting an X-ray. Consequently, atoms of every element emit X-rays during the filling process. Thus, the identity of the atom from which the X-ray was emitted can be established by measuring the amounts of energy present in the X-rays (Skoog, et al. 1997).

2.3.2. Atomic Force Microscope (AFM)

Atomic force microscopy is a surface analysis technique which permits resolution of individual atoms. It is based on the analysis of Van der Waals forces and repulsive forces. An atomically sharp Si based tip scans the surface of a sample interacting with the surface in terms of atomic forces. By using a laser directed onto the tip, the change in the height of the tip is gathered. During the scanning process, an image of the surface giving topographic information is provided by the up-and-down motion of the tip yielding a resolution of a few nanometers. The tip can be moved up and down in one of two modes:

- **Contact mode;** The tip is in contact with the surface. The repulsive forces between the tip and the surface are considered during the scan. Inspite of the possibility of damage the surface during scan, contact mode gives better performance for wide (large) area scans (>100μm).

- **Tapping mode;** The tip oscillates at a fixed frequency and scans the surface. The amplitude changes in the oscillation frequency are detected. Van der Waals forces play largest role between the tip and the surface of the material. In tapping mode better resolution is observed as compared to contact mode (Skoog, et al. 1997).

CHAPTER 3

EXPERIMENTAL

3.1. Materials

Al and Cu targets, pure silicon wafers and Ge implanted silicon wafers at four different implantation doses were used throughout this study. Ge implanted silicon wafers were obtained from Middle Eastern Technical University (METU). These implanted silicon wafers had Ge concentrations of $1x10^{17}$ cm^{-2}, $1.5x10^{17}$ cm^{-2}, $3x10^{16}$ cm^{-2} and $6x10^{16}$ cm^{-2} .

3.1.1. Silicon

Silicon is a nonmetallic chemical element with the symbol Si and atomic number 14. Silicon is the second most abundant element after oxygen in the earth. Compounds of silicon such as silicondioxide or silicate can be found in the atmosphere, natural waters, many plants, sand and rocks.

The atomic structure of silicon makes it an ideal semiconductor. Thus pure silicon is commonly used for electronic and photovoltaic applications such as producing computer chips, transistors silicon diodes, solar cells, microprocessors and semiconducter devices (Skoog, et al. 1997).

3.1.2. Germanium

In this study, silicon wafer substrates were implanted with germanium ions. Germanium has a diamond-like structure and shows similar chemical and physical properties with silicon. It is a stable element in air and water. Germanium is an important semiconductor material which is used in transistors and integrated circuits. It is also used as an alloying agent to increase the index of refraction of glasses or as substrate wafers for high-efficiency multi-junction solar cells in space applications (Skoog, et al. 1997).

3.1.3. Ion Implantation

Ion implantation (Rimini 1995) is a surface modification technique which enhances some of the physical, chemical and optical characteristics of materials, e.g., electrical type and conductance, mechanical hardness, chemical resistance, light emitting centers formation and catalytic properties of material surfaces. Ion implanted semiconductors with different composition and thickness are widely used in the production of advanced devices for optoelectronic and microelectronic applications. To explain surface properties of these advanced technology materials, analytical techniques with high spatial and depth resolution are needed.

The use of silicon-germanium alloys is becoming increasingly important in the semiconductor technology. Since, in circuits, the integration speed of Si-Ge can be faster than Si itself, Si integrated circuits are doped usually with arsenic, phosphorus, boron, boron difluoride, indium, antimony, germanium, silicon, nitrogen, hydrogen or helium. Ion implantation is the most widely used method to dope silicon with these elements (Rubin and Poate 2003).

Germanium implanted silicon wafers were used in this study. A silicon oxide layer of 250 nm thickness was grown on a single-crystalline p-type (100) Si substrate and than implanted with ^{74}Ge ions at doses of between $1\text{x}10^{16}$ and $1\text{x}10^{17}$ cm^{-2} using an implantation energy of 100 keV. The average distance of the implanted Ge atoms from the surface is about 140 nm which was estimated from secondary ion mass spectrometry (SIMS).

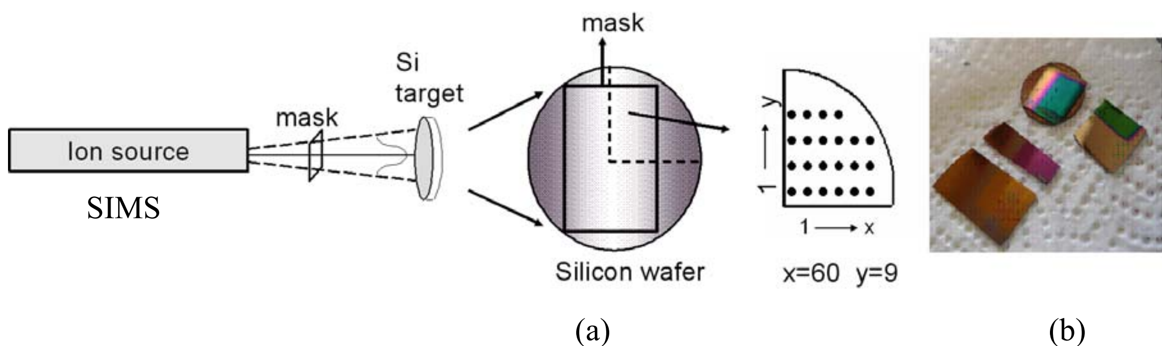

(a) (b)

Figure 3.1. (a) Schematical representation of ion implantation process and (b) a picture of Ge implanted samples (Source: Rimini, et al. 1995 (a))

A schematic representation of the ion implantation process (a) and a picture of Ge implanted samples at different implantation doses (b) are given in Figure 3.1. As shown in the figure, energetic ions were injected into the near-surface region of a substrate through a mechanical mask with a 2x2 cm opening. Ge implanted wafers with different implantation doses on each piece are also shown in Figure 3.1.b. The pink and green colors on the pieces are due to Ge ions diffused out from the mask towards the edges of the target material. Two dimensional (2-D) distribution analyses of the samples were performed starting from the pink region through the green, on wafers of about 1 cm^2 size.

3.2. LIBS Experimental Set-up

All components of the system were purchased from different companies. Then a suitable configuration was choosen and designed in order to conduct LIBS studies. Figure 3.2 shows a scheme of the experimental LIBS set-up used in this work. A Q-switched Nd: YAG laser (Quanta-Ray Lab-170, Spectra Physics, California-USA) operating at 532 nm and emitting pulses of 10 ns duration was focused onto samples at room temperature in air. The energy output was controlled by using a half wave plate/polarizer pair and measured by a powermeter (PE50BB-DIF-V2, Ophir, Israel). The laser beam was passed through 532 nm reflective mirrors (1″ OD, coated, 532 nm reflective, New Focus, Darmstad-Germany) and focused onto the sample surface by different focusing lenses, 17.5 cm (1″ OD, BK7 glass, 440-620 nm, New Focus, Darmstad-Germany), and 10cm (2″ OD, fused silica, CVI, Bensheim-Germany). The sample was placed on an XYZ-translational stage (New Focus, Darmstad-Germany) to change sample position with respect to the laser. Emission from the plasma was collected and imaged by two planoconvex lenses with focal lengths of 10 cm (2″ OD, fused silica, CVI, Bensheim-Germany) and 35 cm (2″ OD, fused silica, CVI, Bensheim-Germany) onto the entrance slit (50μm) of the echelle spectrograph (Mechelle 5000, Andor, f/7, European) and detected by a gated, intensified CCD (ICCD) detector (iStar DH734, Andor Inc., European).

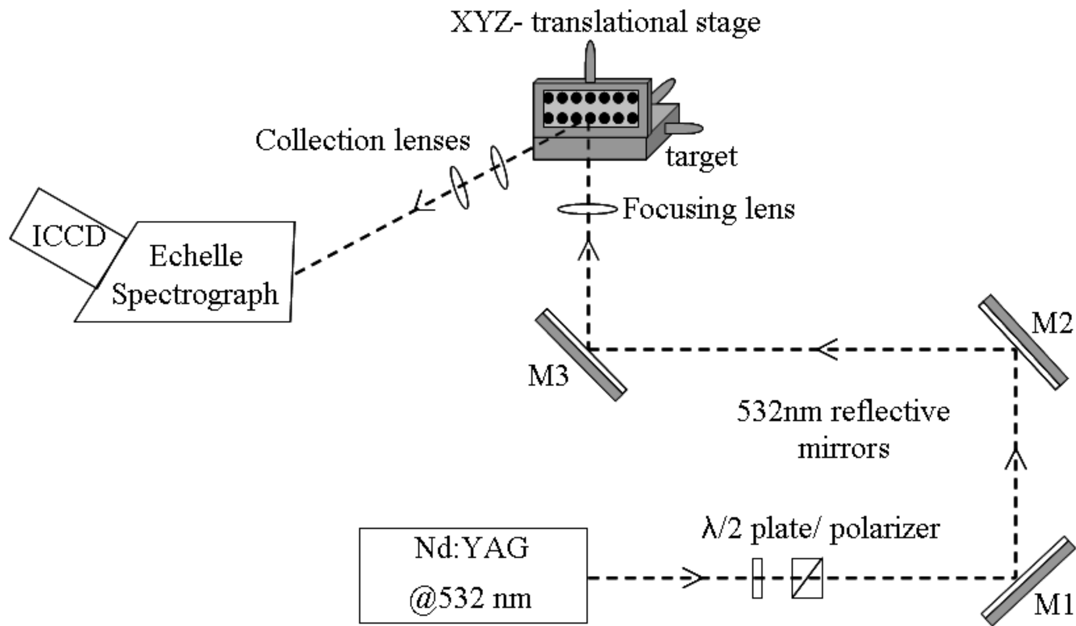

Figure 3.2. Experimental setup for LIBS. M1,M2, M3: reflecting mirrors. ICCD: Intensified Charge Coupled Detector

The spectral range of spectrograph & ICCD is between 200-850 nm with 0.1 nm resolution. Wavelength calibration of the spectrograph was done with a Hg-Ar calibration lamp. Delay time (T_d) and gate time (T_g) of the detector were also optimized. During the experiments a 90 ns delay time and a 1000 ns gate time were used. Specifications of the LIBS system used in this study are also given in Table 3.1.

Table 3.1. LIBS system specifications

LIBS system specifications	
Q-switched Nd: YAG laser	Quanta-Ray Lab-170, Spectra Physics (California-USA)
Half wave plate/polarizer pair	Thorlab SM1PM10 (Newton-New Jersey)
A power meter	PE50BB-DIF-V2, Nova II, Ophir (Israel)
532 nm reflective mirrors	1″ OD, coated, 532 nm reflective (New Focus, Darmstad-Germany)
Focusing lenses	17.5 cm (1″ OD, glass, 440-620 nm, New Focus, Darmstad-Germany) 10cm (2″ OD, fused silica, CVI, Bensheim-Germany)
XYZ-translational stage	New Focus-9067 (Darmstad-Germany)
Collecting lenses	10 cm (2″ OD, fused silica, CVI, Bensheim-Germany) 35 cm (2″ OD, fused silica, CVI, Bensheim-Germany)
Echelle spectrograph	Mechelle 5000, Andor, f/7 (European)
ICCD detector	iStar DH734, Andor Inc. (European)

3.3. SEM/EDX Analysis

After analyzing the surface with LIBS, SEM/EDX characterization was also performed by using a Philips XL-30S FEG type instrument. Images of the sample surfaces were recorded at different magnifications. SEM analysis with back-scatter electron (BSE) detection allows the imaging of materials of different composition at different contrast levels (greyscale/atomic).

Energy-dispersive X-ray Spectroscopy (EDX) analysis was carried out on randomly selected points on the solid surfaces from the region that had shown variation in Ge distribution. SEM measurements allowed the imaging the crater size and morphology of the craters crated by laser shots. However, EDX measurements

permitted the identification of atomic compositions (in atomic percents) of species on the solid samples.

3.4. AFM Analysis

The depth of craters was measured using a Multimode SPM, Nanoscope IV Digital Instrument device type AFM. Measurements were done in contact mode. Sample areas of about 1 cm x 1 cm were used.

CHAPTER 4

RESULTS AND DISCUSSION

4.1. Spectral Analysis by LIBS

In this thesis study, a LIBS system was constructed and applied for spectral compositional analysis of solid samples at İYTE. For that purpose, spectral analysis of some solid surfaces, such as Al, Cu, pure silicon wafer and Ge implanted siliconoxide have been performed.

For qualitative analysis by LIBS, selection of the proper emission line to be used for the identification of each element, is important. For this purpose National Institute of Standards and Technology, NIST Electronic Database were used (NIST 2007) A list of the most intense emission lines observed from Al, Cu, Si and Ge is given in Table 4.1.

Table 4.1. Spectral emission wavelengths of materials used
(Source: NIST)

Element	Wavelength (nm)	Element	Wavelength (nm)
Si (I*)	251.61	Cu (I)	324.75
Si (I)	288.15	Cu (I)	324.89
Si (II)	385.60	Cu (I)	427.51
Si (II)	386.26	Cu (I)	465.11
Si (I)	390.55	Cu (I)	515.32
Si (II)	412.80	Cu (I)	521.82
Si (II)	413.08	Al (I)	309.28
Ge (I)	303.91	Al (I)	309.47
Ge (I)	326.95	Al (I)	394.58
Ge (I)	422.66	Al (I)	396.34

* (I) corresponds to neutral emission lines of elements. Whereas (II) and (III) represents ionic and molecular species, respectively.

LIBS emission spectra obtained from Al and Cu targets within a wide spectral range (250-850 nm) are shown in Figure 4.1 and Figure 4.2, respectively. The inset of each figure shows some prominent lines in detail. Al lines have been measured by using 1.206 mJ/pulse laser energy while 0.983 mJ/pulse laser energy was used for the observation of Cu lines. The spectra were obtained by accumulation of 10 repetetive laser pulses.

In Figure 4.3 emission lines from pure silicon wafer are shown. Spectra was taken with 0.768 mJ/pulse laser energy and a 10 cm focal length lens was used for focusing the beam. The Si-288.15 nm and Si-390.55 nm lines were clearly observed from a single laser shot at 90 ns delay time and 1000 ns gate time.

A Ge-implanted Si wafer surface was also analyzed using LIBS. Figure 4.4 represents the observed Si and Ge lines from a single laser shot with an energy of 1.726 mJ/pulse. Germanium lines observed at Ge (I)-303.91 nm and Ge (I)-326.95 nm have apparently lower signal intensities than those from the silicon matrix lines Si (I) 288.15 and Si (I) 390.55 nm due to the presence of Ge ions with an implantation dose of 1×10^{17} ions/cm^2.

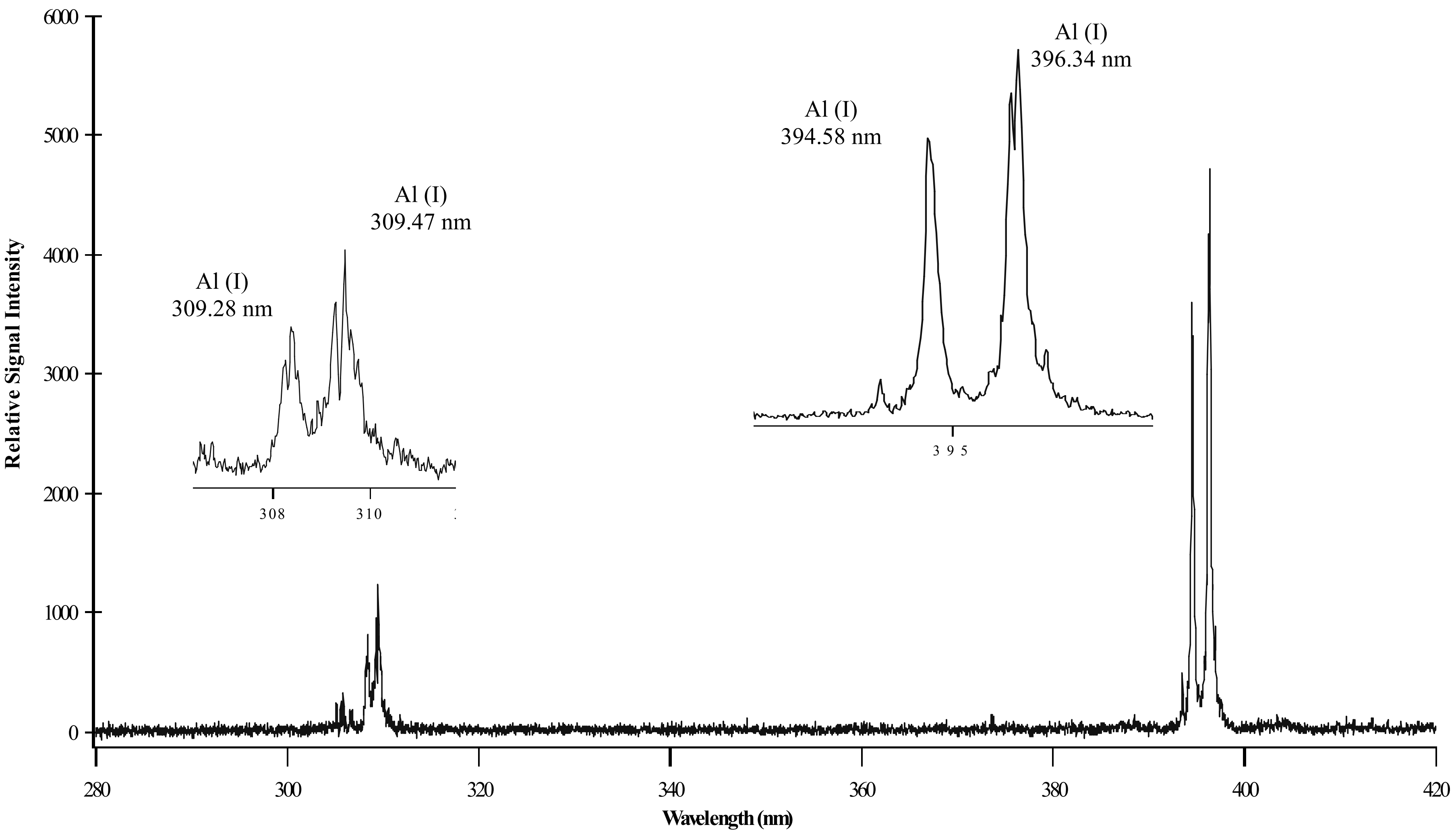

Figure 4.1. Typical LIBS emission spectrum of Al target. 1.206 mJ/pulse laser energy was used and 10 shot accumulation was performed

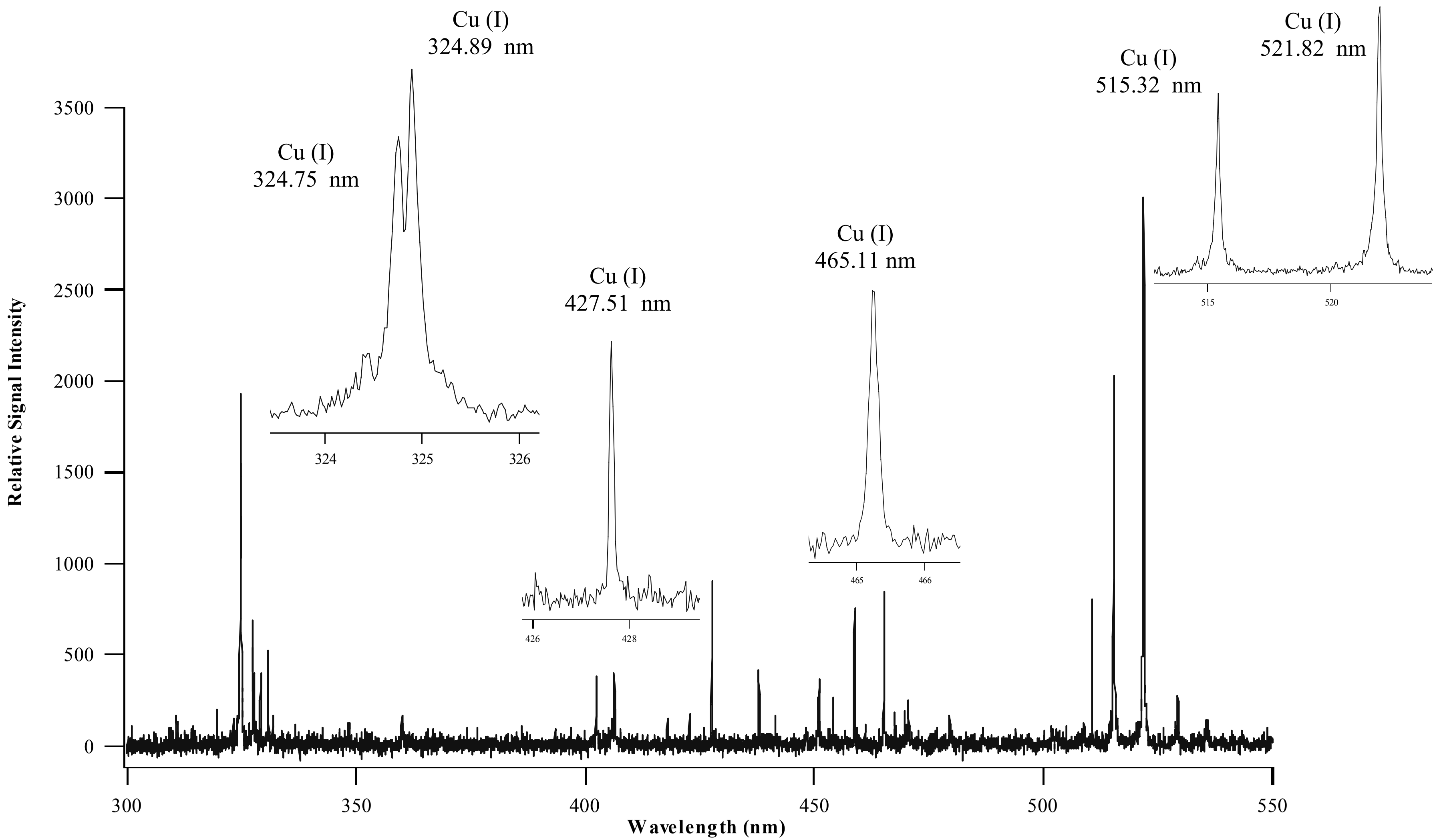

Figure 4.2. Typical LIBS emission spectrum of Cu target. 0.983 mJ/pulse. Fl=17,5 cm, 10 accumulatiıon

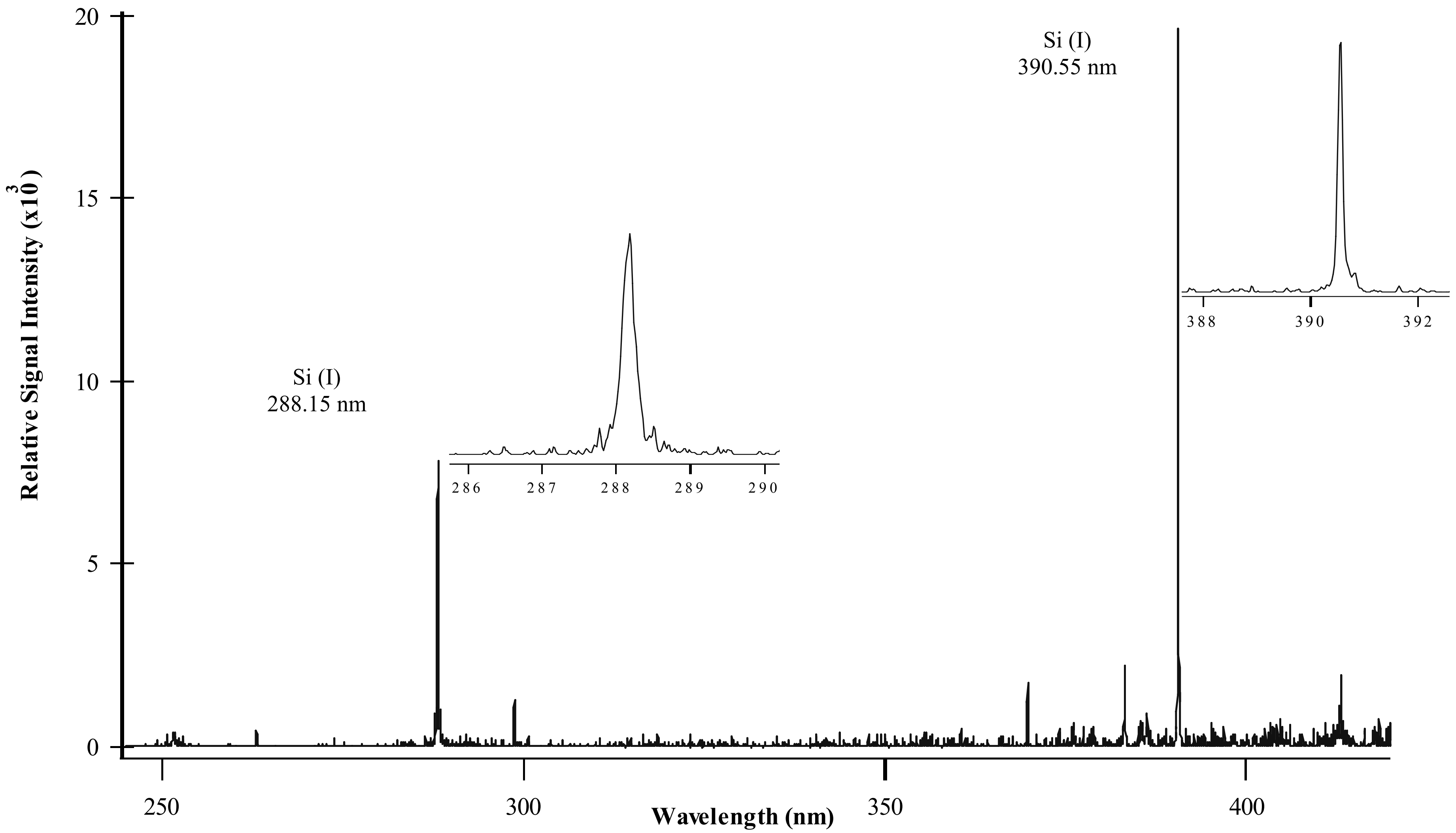

Figure 4.3. Typical LIBS emission spectrum of a pure silicon wafer

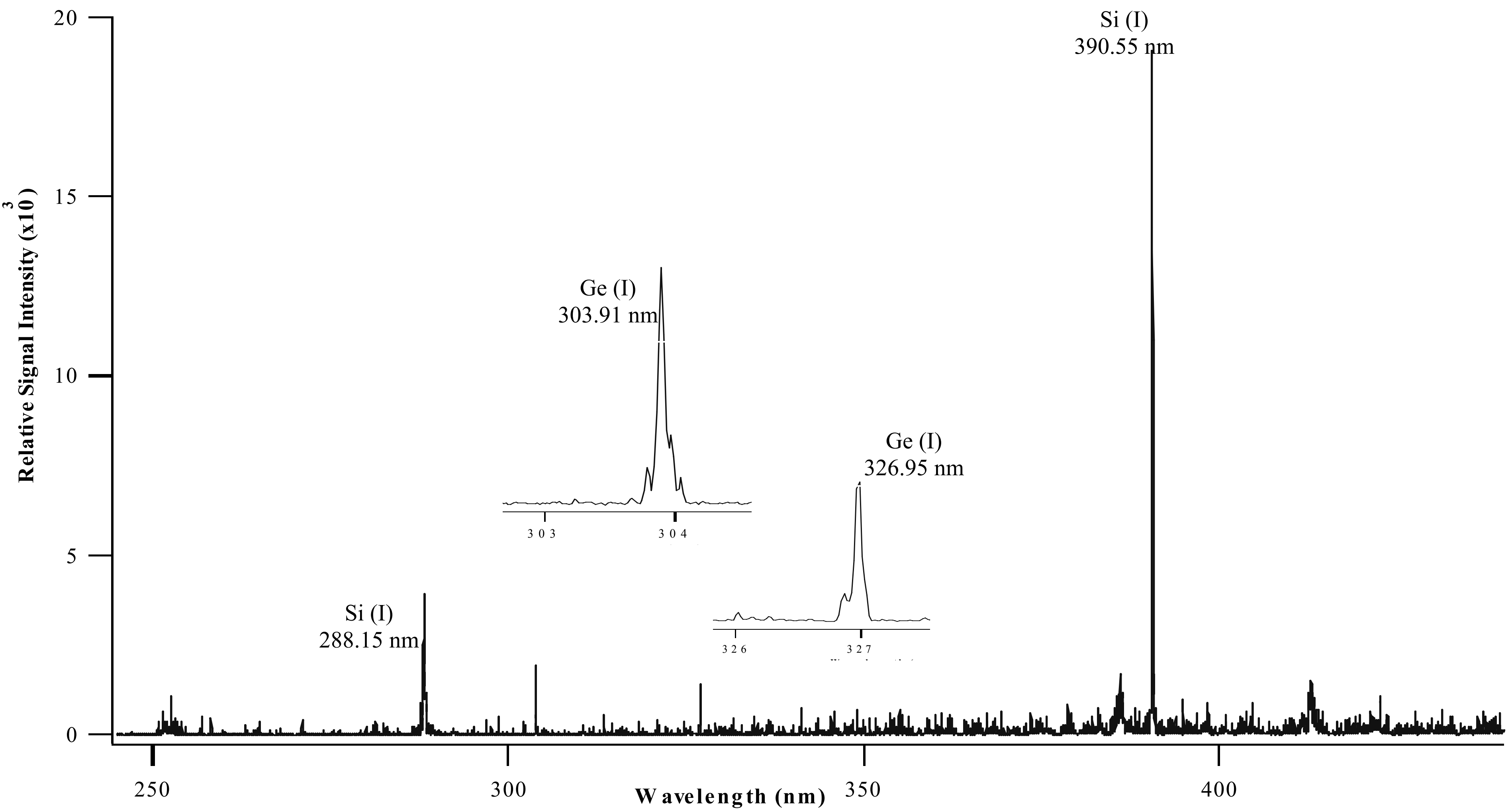

Figure 4.4. Typical LIBS emission spectrum of Ge implanted silicon wafer having an implantation dose of $1x10^{17}$ ion/cm^2

4.2. Signal Optimization

Line emission intensities from the luminous plasma were improved by several signal optimization procedures, such as lens to sample distance, laser energy and the crater size. Time resolution experiments were also performed for 2-D surface and depth profiling analyses.

4.2.1. Focusing Lens to Sample Distance Adjustment

When 2-D compositional mapping analysis is uesed, the smallest possible crater size is required for the best lateral resolution. The minimum spot size on the surface is obtained at the focal point of the lens used. Thus, the distance between focusing lens and sample surface is adjusted to obtain the smallest crater. A micrometer was used to optimize the distance between focusing lens and sample surface. Figure 4.5 reprents the optical microscope images of the craters produced with 17.5 cm focusing lens and single laser pulses of 418 μJ/pulse energy was used. The smallest crater size of 33.88 μm was obtained nearly at the focal point of the lens.

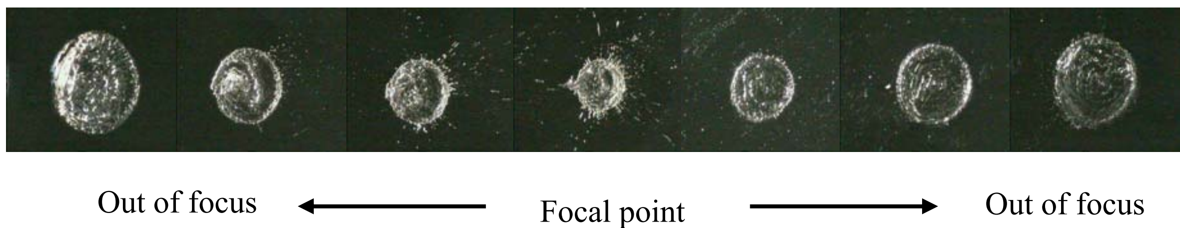

Out of focus ← Focal point → Out of focus

Figure 4.5. Optical microscope images for focusing lens to sample distance adjustment with a 17.5 cm focusing lens and 418 μJ/pulse laser energies on a pure silicon surface, single laser pulses were used

Figure 4.5 shows the variation of LIBS signal intensity with respect to lens position. Normally signal increases as focal position is approached; however, the highest LIBS signal intensity does not always necessarily correspond to the smallest crater size. Therefore, there occurs a compromising condition between the detection limit and the lateral resolution.

On the other hand, in depth profiling analysis, better depth resolution is achieved from craters with the smallest depth. Therefore, the condition that produces the smallest possible crater having the smallest depth with a reasonable LIBS signal was selected for three dimensional (3-D) microanalysis of the surfaces.

4.2.2. Time Resolution

Time resolved spectroscopic measurements were performed in order to find the optimal time window for Ge signal intensity at 303.9 nm by imaging the whole plasma on the entrance slit of the spectrograph. Single shot LIBS spectra of Ge-implanted silicon oxide having an implantation dose of $1x10^{17}$ cm^{-2}, showing the most relevant emission lines, are given in Figure 4.6. The intensities of the ionic and neutral lines of Si and Ge were measured with a time-gate of 1μs, at five different gate delay times: 0, 50, 100, 200 and 400 ns.

Relative signal intensities from the ionic lines of Si (II) at 385.6 nm and 413.11 nm decreased as the gate delay time was increased and disappeared after 200 ns. There was no ionic line emission detected from Ge within this spectral range under these experimental conditions. However, the maximum emission signal from the neutral emission lines of Ge(I) at 303.9 nm and Ge(I) at 326.95 nm were observed after 100 ns delay time with respect to the laser pulse. Strong emission lines from the neutral Si(I) at 288.15 and 390.57 nm were relatively constant up to delay time of 200 ns after which they decreased. Therefore, experiments were conducted with 90 ns delay and 1μs gate time, where maximum Ge line emission observed, for the rest of the study.

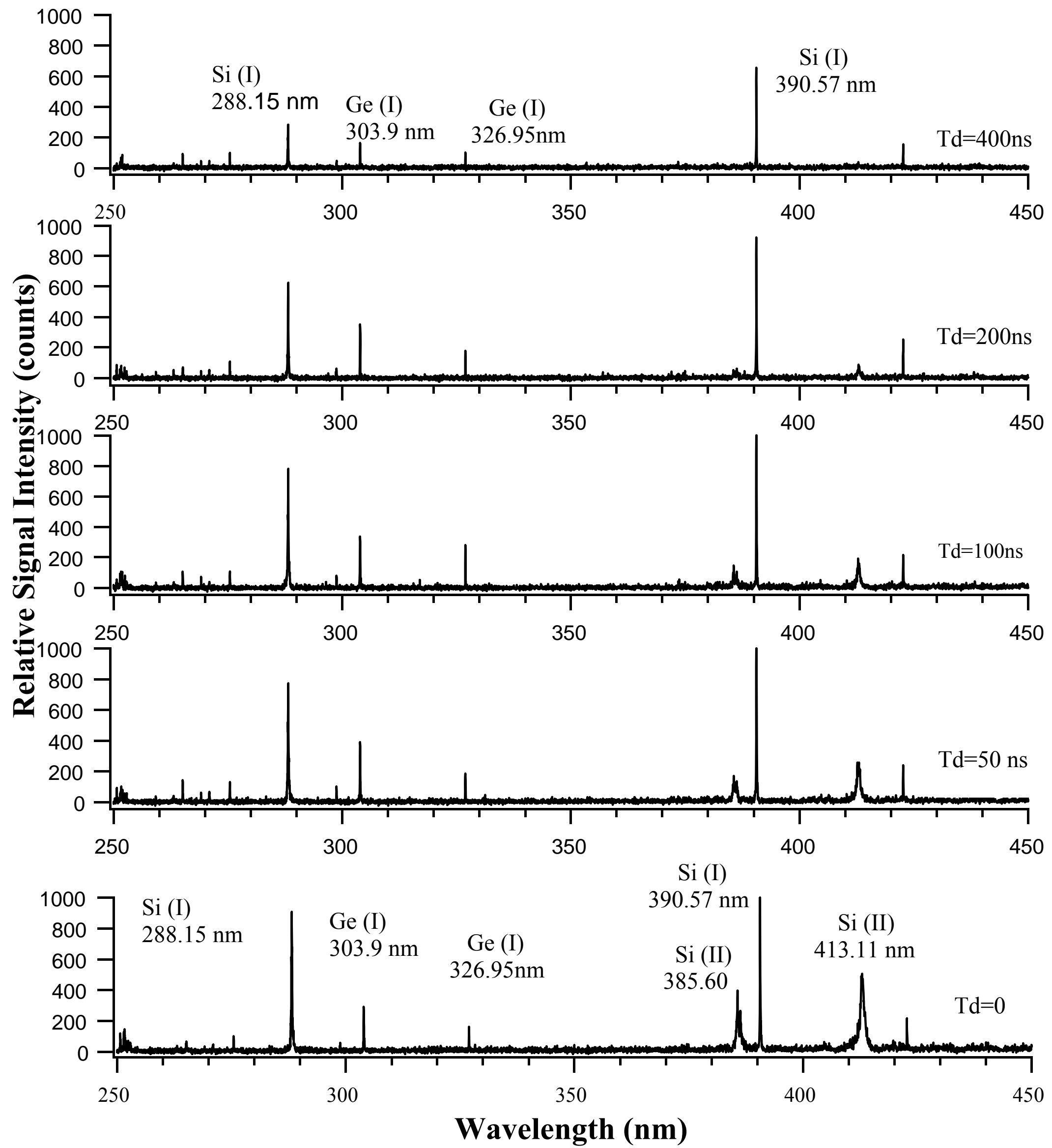

Figure 4.6. Time resolved spectra of Ge implanted samples at several gate delay times with respect to laser pulse. Gate width,Tg, of 1μs laser energy of 1.726 mJ/pulse, 10 cm focusing lens and $1x10^{17}$ ion/cm^2 implantation dose has been used

4.2.3. Germanium Signal Intensity and Implantation Dose

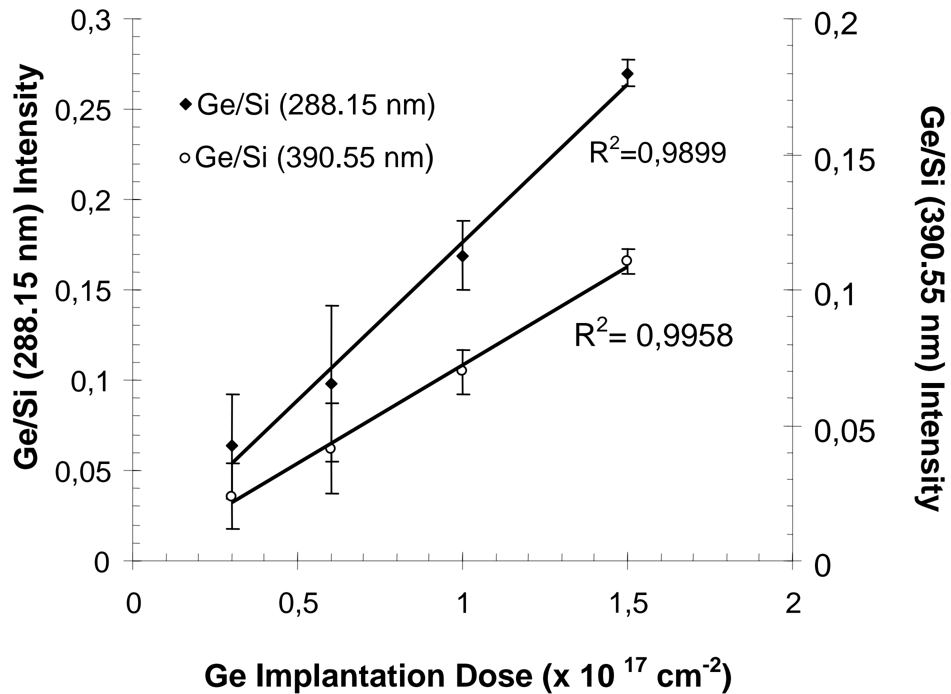

Figure 4.7. Germanium growth curves for Ge (303.9 nm) line, normalized to the 288.15 nm and 390.5 nm Si lines

In order to observe the variation of Ge signal intensity by LIBS with respect to implantation dose, four samples of different implantation dose were used. Ge/Si line intensity ratios plotted against the different Ge implantation doses are shown where the Ge (303.9 nm) line is normalized with respect to neutral Si (288.15 nm and 90.56 nm) lines (Figure 4.7). Each point in the figure represents the average of ten separate single shot samplings from the central part of the implanted region in which a more homogenous distribution exists. Line intensities were obtained from the peak area measurements using a laser energy of 0.69 mJ/pulse. It can be seen from the figure that the normalized Ge intensity exhibits a linear trend with respect to implantation dose with correletaion coefficients of R^2=0.989 and R^2 = 0.995, when normalized to the Si- 288.15 nm and 390.5 nm line emissions, respectively. The percent relative standard deviation (% RSD) of the measurements ranged from 10–25% and relatively high

regression constant values indicated the possibility of semi-quantitative analysis of ion implanted surfaces by LIBS.

4.2.4. Effect of Laser Energy

When nanosecond laser pulses are focused onto a target surface, the absorbed energy heats up the target to the melting point and then to the vaporization temperature. The power density is high enough that melted material is ejected due to the plasma pressure, with plasma plume expanding into the ambient atmosphere. The ablated amount from the surface is largely dependent on the incident laser energy.

The energy of the laser was tuned by using a half wave plate/polarizer pair and plasma emission was collected using a side-viewing configuration, by imaging the plasma onto the entrance slit of the spectrograph. The effect of laser energy on laser induced plasma emission intensity is given in Figure 4.8. Here, spectra from the pure silicon wafer were recorded within the 250-850 nm spectral regions for energies of 56 µJ - 1.7 mJ/pulse. This energy range corresponds to 0.38 GW/cm^2 – 11.5 GW/cm^2 irradiance values for crater sizes of 43 µm. The diameter of the focused beam size, d, was calculated from the equation (Laserna 2004);

$$d = 2.44 * \lambda * f / D \qquad (1\text{-}1)$$

where λ is the laser wavelength (532 nm), f is the focal length of the lens (100 mm) and D is the diameter of the collimated laser beam (3 mm, after aperture).

A time delay of 90 ns and gate width of 1µs gave the maximum LIBS signal for the Si lines. After that, 90 ns and gate width of 1µs were used in all experiments. Peak areas calculated from three separate single shot measurements at each laser energy were used to construct the figure for neutral Si (I) lines at 288.15 nm and 390.5 nm (Figure 4.8).

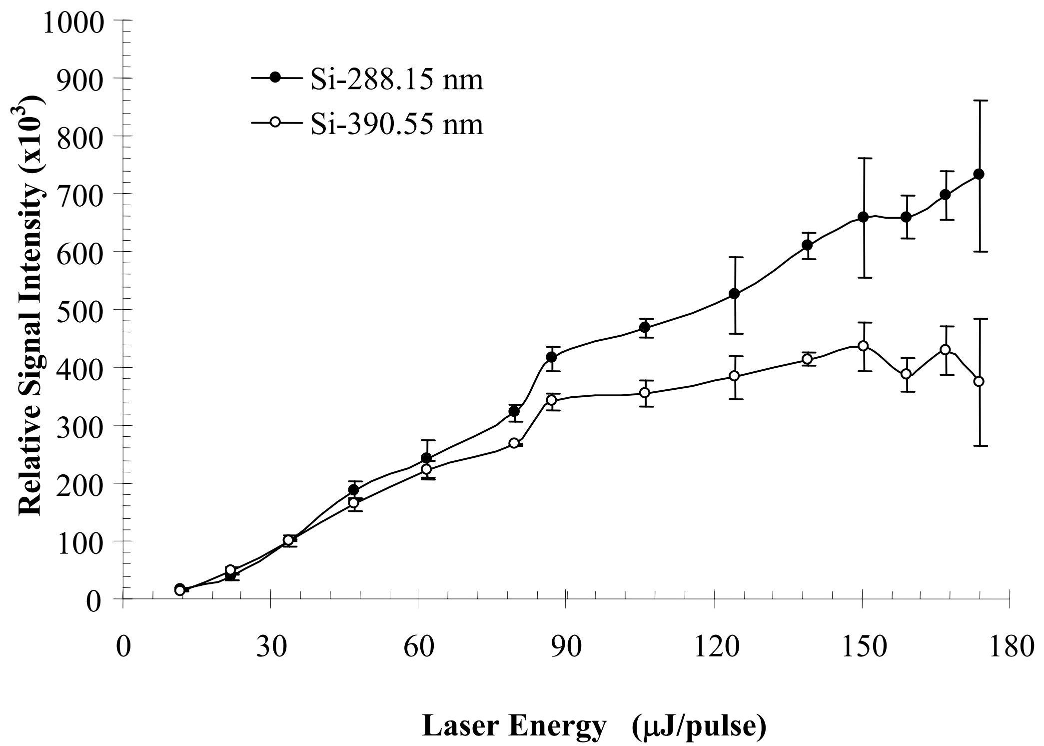

Figure 4.8. Relative signal intensities of Si–288.15 nm and Si–390.55 nm at different laser energy. The pure silicon wafer has been analyzed with a 10 cm focusing lens and one single laser shot

Generally signal intensity increases as the laser energy increases. For both Si-288.15 nm and Si-390.55 nm lines signal intensity deviates from linearity at high energies (>50 μJ/pulse), which could be attributed to laser beam absorption by the plasma above the target surface known as plasma shielding (Aguilera 1998, Russo 2004). However, in the region between 56 μJ/pulse and 80 μJ/pulse 2 different regions were observed. Initially a sharp increase in signal intensity was observed between 56-60 μJ/pulse energy, then it slows down and bends between 60- 80 μJ energy range. Then, a second increase in signal intensity between 80-90 μJ/pulse energy is observed. Finally, signal emission rolls off drastically, after 90 μJ/pulse laser energy. This variation in signal intensity within this power regime (0.38 GW/cm^2 – 11.5 GW/cm^2) could be explained by the evolution of the plasma at different irradiance regimes (Root 1989, Yalcın 1999).

Two dimensional (2-D) scanning analysis measurements were performed at low pulse energies of between 56-250 μJ where the signal emission is mostly due to the neutral and singly ionized atoms. In this regime, the plasma has a low temperature and low electron density and is thin enough to allow the laser radiation to penetrate for proportional ablation (Yalcin, et al. 1999)

4.2.5. Crater Size

As mentioned in the previous section, the low energy laser pulses produce small craters and hence better lateral and depth resolution on solid surfaces is achieved. In order to investigate the variation of crater size with respect to laser energy, SEM images of craters produced at various laser energies were analyzed. Figure 4.9 shows the corresponding SEM pictures. At low laser energies there is less damage compared to high laser energies. Increasing laser energy results in splashing of the ablated material while the plasma plume expands into the atmosphere contaminating the edges of the crater.

The size of the craters increases logarithmically as pulse energy increases and rolls off after 500μJ pulse energy (Figure 4.10). This shows when the shielding of the material surface by the intense plasma has occured, the plasma may absorb incident energy after it is formed during the laser pulse by shielding the target surface from the laser beam. Therefore, a decrease in ablated material is observed.

The decrease in the ablation rate (saturation in mass removal) at high fluences could also explain the observed decrease in signal intensity (Yalcin, et al. 1999). Also, the observed decrease in signal intensity for 390.5 nm Si (I) line, is much more severe compared with that of 288.15 nm Si (I) line.

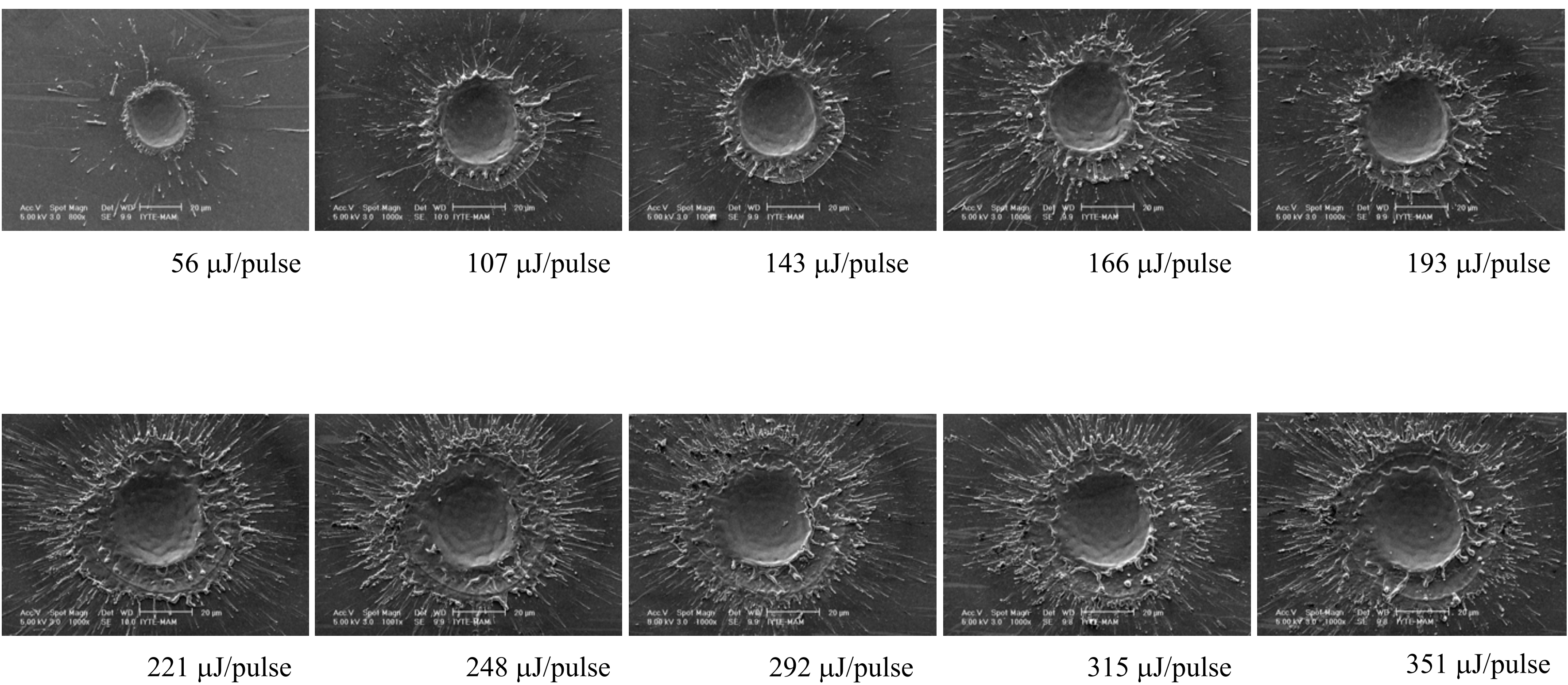

Figure 4.9. SEM images of the craters that were obtained by a single laser shot with 10 cm focusing lens at different laser energies

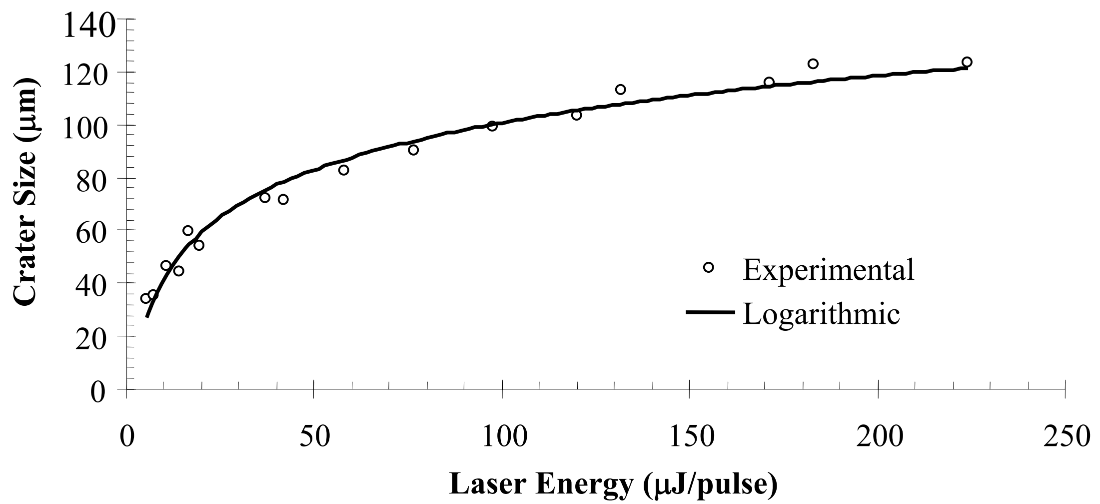

Figure 4.10. Relationship of laser energy to crater size. The pure silicon wafer has been analyzed with a 10 cm focusing lens and a single laser shot at each laser energy

4.3. Two Dimensional (2-D) Compositional Mapping

4.3.1. LIBS Analysis

In the case of 2-D scanning analysis of the surfaces for determination of the compositional variation of the element of interest, the lateral resolution is the main issue to be considered. High lateral resolution can be obtained by using the smallest focal spot possible and the lowest pulse energy, which gives rise to a detectable LIBS signal (Bette and Noll 2003).

Low energy laser pulses can provide high lateral resolution at the expense of sensitivity. Figure 4.11.a shows an SEM photomicrograph of the 2-D scanning analysis of the Ge-ion implanted Si wafer surface within an area of 1.6 x 12 mm . Sixty craters have been created on each of 9 rows with 5 laser shots each, at a laser energy of 250 μJ/ pulse. All representative image of a single crater formed by 5 consecutive laser shots is given in Figure 4.11.b.

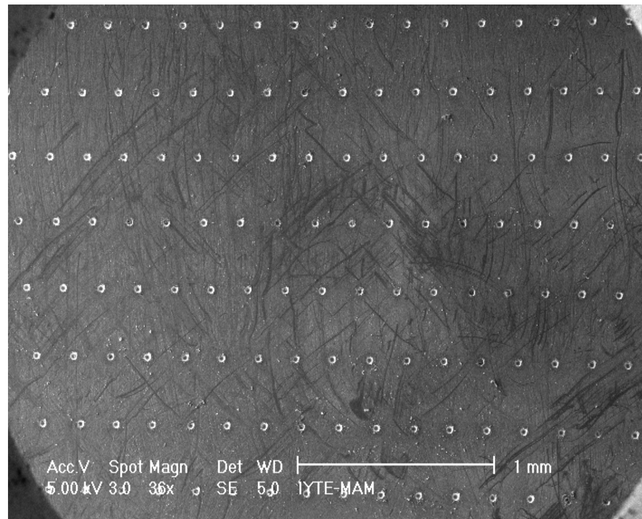

(a)

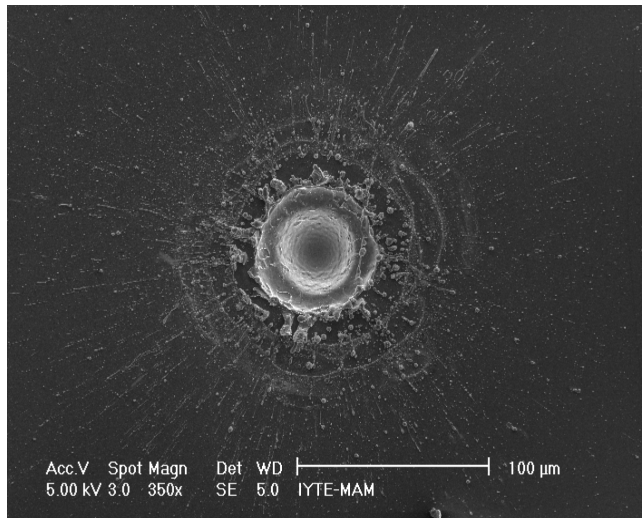

(b)

Figure 4.11. (a) SEM image of the Ge-ion implanted Si wafer within an area of 1.8 x 12 mm^2 60 craters have been constructed on each 9 rows with 5 laser shot by a laser energy 250 µJ/ pulse (b) The image of a single crater formed by 5 consecutive laser shots

When a 3-D graph of this scanning was plotted against the Ge signal intensity at Ge (I) 303.9 nm (Figure 4.12), the variation in Ge intensity can be observed. The scanning was begun from a point on which there was no implanted Ge ion present. Laser pulses of 250 µJ/ pulse energy were used on samples having a Ge implantation dose of $6x10^{16}$ cm^{-2}. A 12x1.6 mm (x:y) sampling area starting from the outer edge representing low Ge concentration diffused out of the mechanical mask, (see Figure 3.1.b) to the center of the implanted region was scanned at 200 micrometer

intervals. There were nine rows of sampling on the vertical (y) axis, each containing 60 sequentially formed craters. Here, only 4 of the 9 series in vertical axis are shown in the Figure 4.12.a for clarity. LIBS spectral measurements revealed low Ge concentrations at the edge and higher concentrations toward the center of the implanted region.

The distribution shown in the forefront Figure 4.12.b was obtained from the non-implanted region of the SiO_2 surface (blank), whereas the one at the back was obtained from the implanted region. Lower pulse energies of 69 microjoules enabled the sampling of 50 micrometer intervals. The same high noise characteristics observed for both implanted and non-implanted regions can be attributed to the use of the ICCD detector at high gain settings.

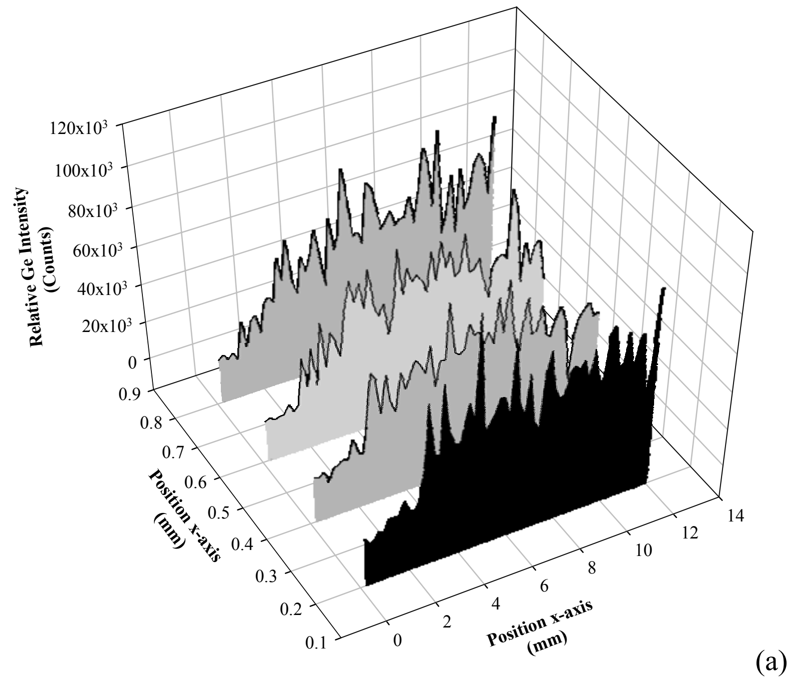

(a)

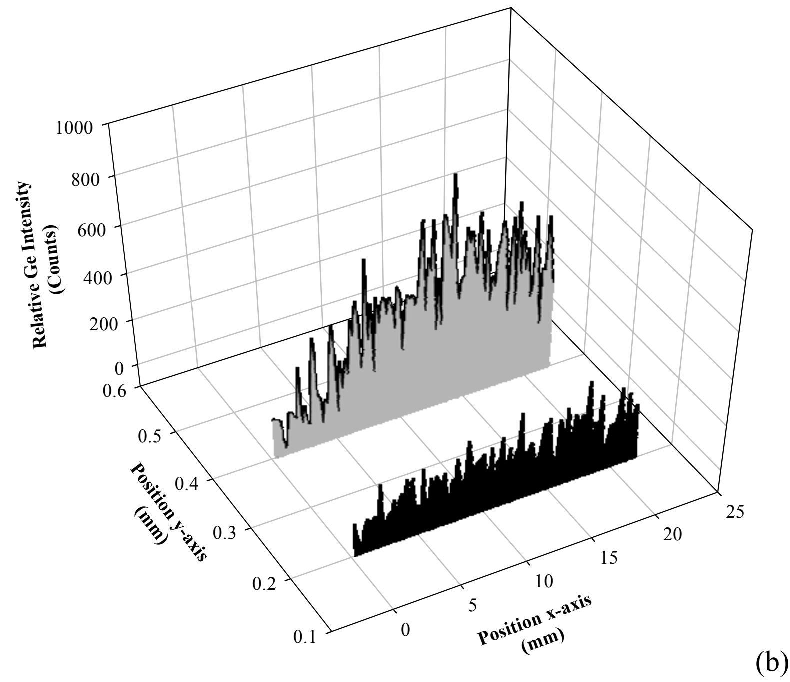

(b)

Figure 4.12. Ge ion distribution on implanted SiO_2 surfaces. (a) 250 μJ/pulse energy, 200 μm sampling intervals in both (x:y) direction, (b) 69 μJ/ pulse energy, 50 μm sampling intervals, from implanted region (back) and non-implanted region (front)

Figure 4.13 shows a contour map of the 2-D Ge-ion distribution from the LIBS measurements. Within a 12 x 1.6 mm sampling area, with 200 µm intervals, a total of 540 LIBS measurements were performed and analyzed at the neutral 303.9 nm Ge (I) emission line. Intensities obtained from the peak area of the Ge (I) lines were plotted as a contour graph in counts (arbitrary units).

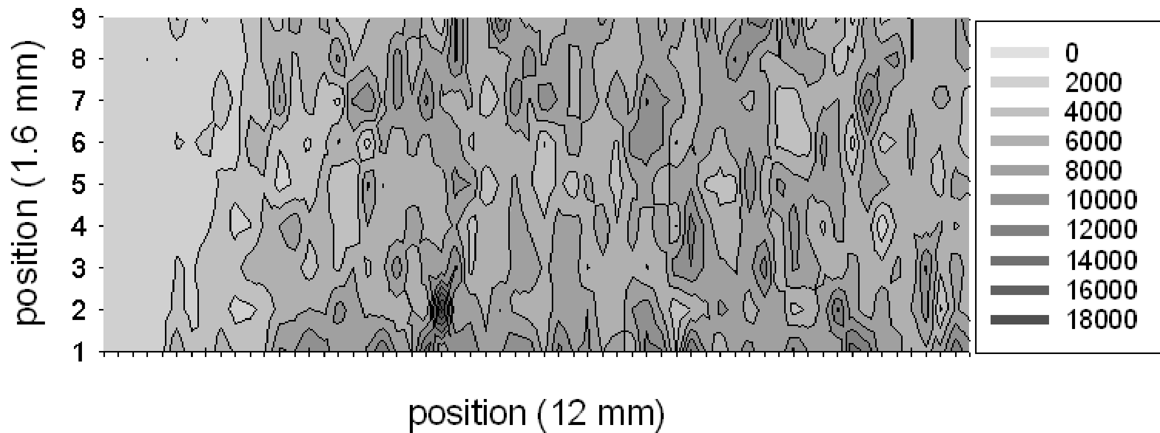

Figure 4.13. Contour plot showing the 2-D Ge ion distribution on SiO_2 matrix. Darker colours represent a higher concentration of Ge ions. 250 µJ/pulse energy, 200 µm sampling intervals in both (x:y) direction

4.3.2. SEM/EDX Analysis

The morphology and size of the ablated spots on the Si wafers were investigated by SEM. The smallest crater size from a single laser pulse of 0.056 mJ energy was measured as 33.88 µm in diameter, from edge to edge of the ablated spot, and is shown in Figure 4.14.

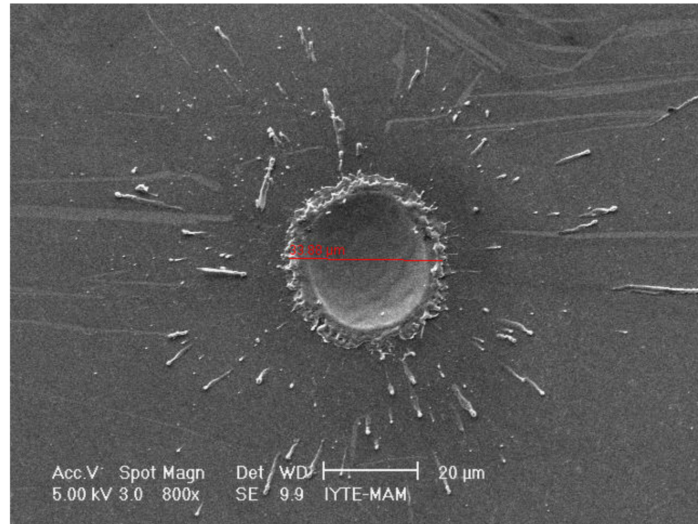

Figure 4.14. SEM image of a 33.88 μm crater that has been obtained from a single laser shot of 56 μJ laser energy. A 10 cm focusing lens was used to focus the laser beam onto a pure silicon wafer

Energy dispersive X-ray (EDX) spectrometry can be used to evaluate the elemental distribution of the surfaces, as an integrated feature of scanning electron microscopy, (SEM). In this study, in order to compare with LIBS spectral measurements, SEM-EDX was used to determine Ge, Si and O atomic percentages of various implantation dose samples. Measurements were performed on the areas where the highest Ge ion distribution was present. Table 4.2 contains the average of five consecutive measurements for each implantation dose. A regression constant of R^2=0.948 was obtained from a calibration graph drawn for the range of concentrations considered. It can be seen that atomic percent concentrations of Ge ions increases, from 1.58% to 5.27%, while oxygen and silicon content remain almost constant as implantation dose increases.

Table 4.2. SEM-EDX measurements, atomic percent values for Si, Ge and O atoms at different implantation doses. Data were obtained from five different measurements ($R^2 = 0.948$)

Implantation Dose	Atomic % Oxygen	Atomic % Germanium	Atomic % Silicon
3.0×10^{16}	32.77	1.58	65.64
6.0×10^{16}	30.77	2.36	66.87
1.0×10^{17}	37.87	4.49	57.64
1.5×10^{17}	32.56	5.27	62.18

In order to compare 2-D scanning LIBS analysis with EDX, line scan analysis of implanted surfaces by SEM-EDX was also performed. Lateral analysis by EDX was performed by starting from the edge to the center of the implanted region in a way similar to how it had been done for LIBS measurements. A sample with a 6×10^{16} Ge ions/cm^2 implantation dose was used for line scan analysis and elemental compositions of Si, O, and Ge ions were obtained.

Figure 4.15 represents the elemental distribution of Si, Ge and O atoms measured at 60 different positions at about 200 μm intervals, along the horizontal axis (x-axis). In this figure, the Ge atomic percentage values obtained from EDX measurements are shown on the right y-axis while Si and O were on the left. It was observed that Ge ion concentration changes, laterally, from (0.5-2.8) % (atomic) for a sample with 6×10^{16} cm^{-2} implantation dose. This range was estimated as (0.2-1.58) % when 3×10^{16} Ge ions/cm^2 implantation dose of a sample was used. Each point in the figure is the average of 5 consecutive measurements. It can be seen that the atomic percent concentrations of Ge ions increases while oxygen and silicon remains almost constant as implantation dose increases.

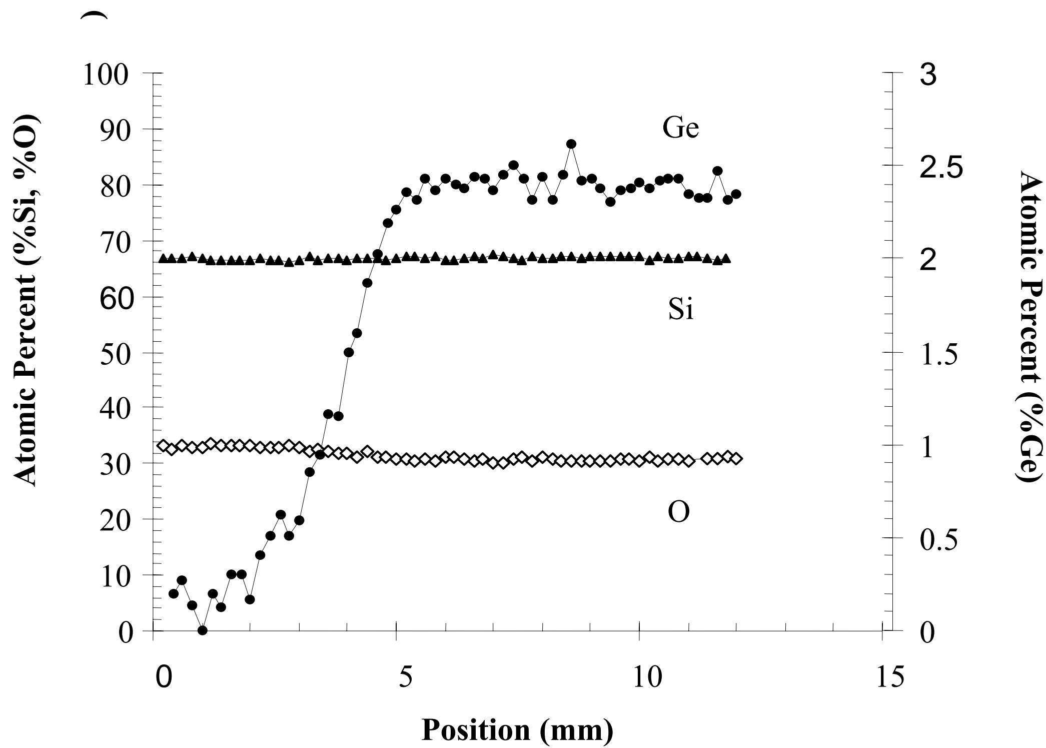

Figure 4.15. SEM-EDX line scans analysis for Ge ion distribution. $6x10^{16}$ Ge ions/cm^2 implantation dose were used and the sample was scanned from the edge through the center of the implanted region

4.4. Depth Analysis

4.4.1. AFM Analysis

Atomic force microscopy (AFM) has the ability to make measurements in both lateral and vertical dimensions. In this study, AFM was utilized to get information about surface topography and depth of the laser-generated craters.

An AFM image of a crater produced by a single laser pulse of 50 μJ energy is given in Figure 4.16.a. In addition, the depth profile obtained from this measurement is presented in Figure 4.16.b. As it can be seen from the figure, the crater was 30 μm in diameter and 800 nm in depth. The weight of ablated material was calculated by assuming the crater has a semi-spherical ($A= \pi r^2 h$) shape and it was found to be 5.26 ng.

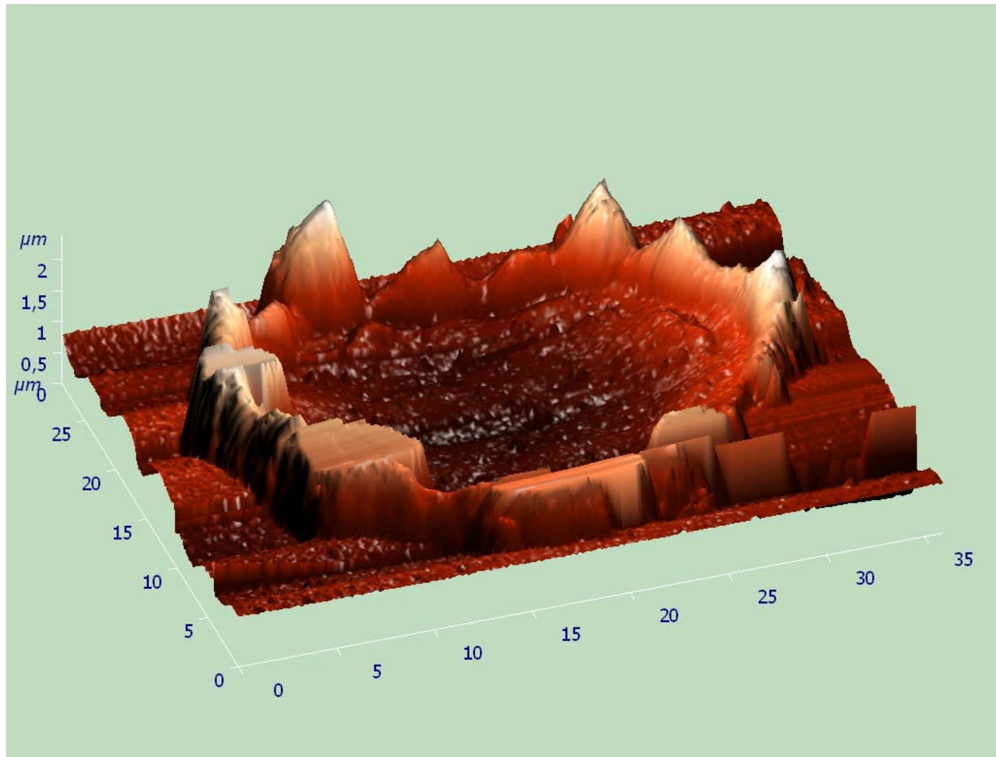

(a)

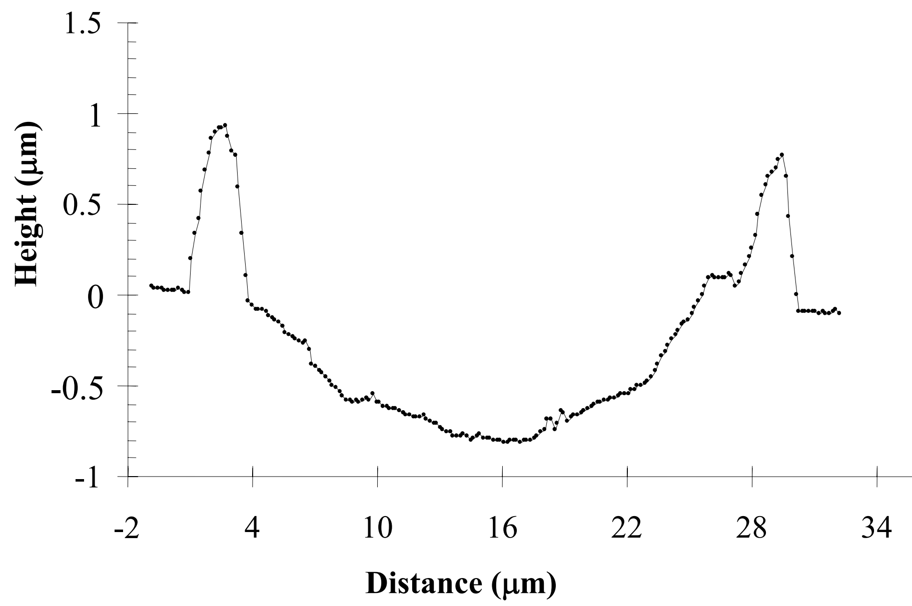

(b)

Figure 4.16. (a) Atomic force microscope image and (b) depth profile of a crater formed from a single laser shot with 50 µJ/ pulse energy

4.4.2. LIBS Spectral Analysis

The shallowest crater depth obtained from the lowest energy (69μJ) laser pulse, that can produce an observable LIBS emission signal, was given in the previous section from AFM measurements, as 800 nm. Also the depth of the silicon oxide layer used in this study in which Ge ions had been implanted was previously determined to be 250 nm. Therefore, this was the lowest pulse energy that was able to ablate a 200 nm deep SiO_2 layer from a single shot. This is the limiting factor of the present experimental configuration that prevents performing depth profiling measurements (in vertical direction) of Ge ions within this scale (200 nm). This was verified from LIBS spectral measurements of the Ge (303.9 nm) and Si (288.15nm) line intensities from multiple shot measurements. Spectral line emission intensity from ten sequential laser pulses on the same spot were saved separately, and accumulated afterwards with respect to shot number. Data presented in Figure 4.17 shows constant line emission intensity from the Ge 303.9 nm line after the second shot, whereas the accumulated signal intensity from the Si 288.15 nm line increases as the shot number increses, which indicates the removal of the Ge implanted layer after the second shot. Statistical error analysis was also performed from three replicate measurements.

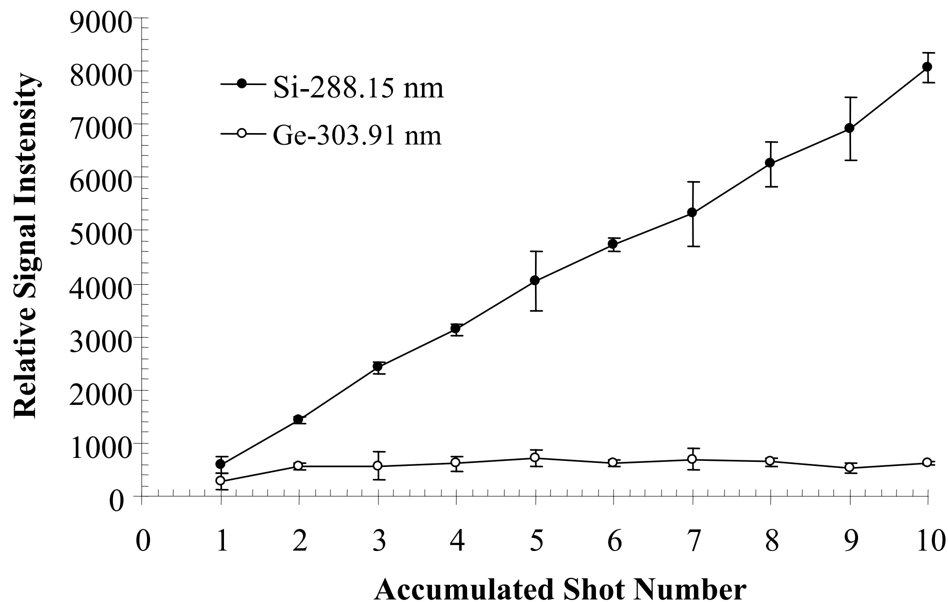

Figure 4.17. Relative intensities of Si -288.15 and Ge -303.91 nm lines with respect to increasing number of laser pulses

CHAPTER 5

CONCLUSIONS

LIBS has been demonstrated as a semi-quantitative spectral analysis technique for 2-D analysis of Ge-implanted silicon oxide surfaces. A typical LIBS optical system was designed, constructed from its commercially available parts for solids analysis at İYTE. Germanium -samples with implantation doses of between $1x10^{16}$-$1.5x10^{17}$ ions/cm^2, prepared by the method of ion implantation were analyzed for the the assessment of the LIBS system constructed.

LIBS spectral measurements indicate 50 µm lateral and 800 nm depth resolution from single shot measurements. SEM-EDX analysis has been used to correlate semi-quantitative LIBS spectral measurements. It has been shown that LIBS has the capability to detect atomic concentrations of Ge ions lower than 0.2% in the Si/SiO_2 matrices.

For two dimensional (2-D) scanning analysis LIBS presents advantages over SEM-EDX analysis in terms of scan time, but has similarities in both accuracy and sensitivity. It can be concluded that lateral and depth resolution can be further improved by the establishment of tighter focusing of the laser beam and gentler ablation conditions with the use of less energetic laser pulses.

REFERENCES

Aguilera, J.A., Aragon, C., Penalba, F., 1998. Plasma shielding effect in laser ablation of metallic samples and its influence on LIBS analysis. *Applied Surface Science* 127: 309-314.

Andor Technology, Digital Camera Fundamentals Rank Top 2 http://www.andor.com/library/digital_cameras (accessed September 30, 2007).

Bärsch, N., Körber, K., Ostendorf, A., Tönshoff, K.H., 1996. Ablation and cutting of planar silicon devices using femtosecond laser pulses. *Applied Physics* 77(A):237-242.

Bette, H., M.F., Noll, R., 2003. High-speed scanning laser-induced breakdown spectroscopy at 1000 Hz with single pulse evaluation for the detection of inclusions in steel. *Applied Physics* 37:1281– 1288.

Brennetot, R., Lacour, J.L., Vors, E., Rıvoallan, A., Vaılhen, D., Maurıce, S., 2003. Mars Analysis by Laser-Induced Breakdown Spectroscopy (MALIS): Influence of Mars Atmosphere on Plasma Emission and Study of Factors Influencing Plasma Emission with the use of Doehlert Designs. *Applied Spectroscopy* 57:744–752.

Bustamante, M.F., Rinaldi, C.A. and Ferrero, J.C., 2002. Laser induced breakdown spectroscopy characterization of Ca in a soil depth profile *Spectrochimica Acta Part B* 57:303–309.

Cravetchi, I.V., Taschuk, M.T., Tsui, Y.Y., Fedosejevs, R., 2004. Scanning microanalysis of Al alloys by laser-induced breakdown spectroscopy *Spectrochimica Acta Part B* 59:1439–1450.

Dixon, P.B., Hahn, D.W., 2005. Feasibility of detection and ıdentification of ındividual bioaerosols using laser-ınduced breakdown spectroscopy. *Analytical Chemistry* 77:631–638.

Dolores, R., Lasrena, J.J., 1998. Surface and tomographic distribution of carbon impurities in photonic-grade silicon using laser-induced breakdown spectrometry. *Journal of Analytical Atomic Spectrometry* 13:557–560.

García, C.C., Corral, M., Vadillo, J.M. and J. J. Laserna, 2000. Angle-Resolved Laser-Induced Breakdown Spectrometry for Depth Profiling of Coated Materials. *Applied Spectroscopy* 54:1027-1031.

Giakoumaki, A., Melessanaki, K., Anglos, D., 2007. Laser-induced breakdown spectroscopy (LIBS) in archaeological science applications and prospects. *Analytical Bioanalytical Chem*istry 387:749–760.

Gondal M.A., Hussain, T., Yamani, Z.H., Baig, M.A., 2006. The role of various binding materials for trace elemental analysis of powder samples using laser-induced breakdown spectroscopy. *Talanta* 72:642–649.

Häkkänen, H., Houni, J., Kaski, S., Korppi-Tommola, J.E.I., 2001. Analysis of paper by laser-induced plasma spectroscopy. *Spectrochimica Acta Part B* 56: 737-742.

Knight, A.K., Scherbarth, N.L., Cremers, D.A., Ferrıs, M.J., 2000. Characterization of Laser-Induced Breakdown Spectroscopy (LIBS) for Application to Space Exploration. *Applied Spectroscopy* 54:331–340.

Laserna, J.J., Vadillo, J.M., 2004. Laser-induced plasma spectrometry: truly a surface analytical tool. *Spectrochimica Acta Part B* 59:147–161.

Margetic, V., Bolshov, M., Stockhaus, A., Niemax, K., Hergenröder, R., 2001. Depth profiling of multi-layer samples using femtosecond laser ablation. *Journal of Analytical Atomic Spectrometry* 16:616-621.

Mateo, M. P., Nicolas, G., Pinon V. and A. Yanez, A., 2006. Improvements in depth profiling of thick samples by laser-induced breakdown spectroscopy using linear correlation. *Surface Interface Analysis* 38:941–948.

Mateo, M.P., Vadillo, J.M., Laserna, J.J., 2001. Irradiance-dependent depth profiling of layered materials using laser-induced plasma spectrometry. *Journal of Analytical Atomic Spectrometry* 16:1317-1321.

Milan, M., Lucena, P., Cabalin, L.M., Laserna, J.J., 1998. Depth Profiling of Phosphours in Photonic-Grade Silicon Using Laser-Induced Breakdown Spectrometry. *Applied Spectroscopy* 52:444-448.

Mirov S.B., Pitt, R.E., Dergachev, A., Lee, W., Martyshkin, D.V., Mirov, O.D., Randolph, J.J., DeLucasc, L.J., Brouillette, C.G., Basiev, T.T., Orlovskii, Y.V. Alimov, O.K., 1999. A novel laser breakdown spectrometer for environmental monitoring. *Society of Photo-Optical Instrumentation Engineers* 3855: 34–41.

NIST Atomic Spectra Database Lines Form
National Institue of Standards and Technology
http://physics.nist.gov/PhysRefData/ASD/lines_form.html
(accessed September 25, 2007).

Pronko, P.P., Dutta, S.K., Du, D., 1995. Thermophysical effects in laser processing of materials with picosecond and femtosecond pulses. *Journal of Applied Phys*ics 78:6233-6240.

Radziemski, L.J., Cremers, D.A., 1989. *Handbook of Laser-Induced Breakdown Spectroscopy*. New York: Marcel Dekker, Optical Engineering Series.

Rieger, G. W., Taschuk, M., Tsui, Y.Y., Fedosejevs, R., 2002. Laser Induced Breakdown Spectroscopy for Microanalysis Using Submillijoule UV Laser Pulses. *Applied Spectroscopy* 56:689-698.

Rimini, E., 1995. *Ion Implantaion Basics to Device Fabrication*. Boston: Kluwer Academic Publishers.

Root, R.G., 1989. *Laser Induced Plasmas and Applications*. New York: Marcel Decker.

Rubin, L., Poate, J., 2003. *Ion Implantation in Silicon Technology*. New York: American Institute of Physics.

Russo, R.E., Mao, X.L., Liu, C., Gonzales, J., 2004. Laser assisted plasma spectrochemistry: laser ablation. *Journal of Analytical Atomic Spectrometry* 19:1084-1089.

Samek, O., Telle, H.H., Beddows, D.C.S., 2001. Laser-induced breakdown spectroscopy: a tool for real-time, *in vitro* and *in vivo* identification of carious teeth. *BMC Oral Health* 1(1)6831-1472.

Sauter, E.G., 1996. *Nonlinear Optics*. New York: John-Wiley.

Siegman, A. E., 1986. *Lasers*. California: Sausalito,University Science Books.

Silfvast, W. T., 1996. *Laser fundamentals*. Cambridge; Cambridge unv. Press.

Skoog, D.A., Holler, and F.J., Nieman, T.A., eds. 1997. *Principles of Instrumental Analysis*. New: York Hardcover .

Skoog, M.D., West, D.M., and Holler, F.J., eds. 1997. *Fundamentals of Analytical Chemistry*. Florida: Harcourt Brace & Company.

Sneddon J., Thiem T.L., and Lee Y-III., eds. 1997. *Lasers In Analytical Atomic Spectroscopy*. New York: VCH Publishers.

Vadillo, J.M., Garcia, C.C., Palanco, S., and Laserna, J.J., eds. 1998. Nanometric range depth- resolved analysis of coated-steels using laser-induced breakdown spectrometry with a 308 nm collimated beam. *Journal of Analytical Atomic Spectrometry* 13:793-797.

Winefordner, J.D., Gornushkin, I.B., Correll, T., Gibb, E., Smith, B.W., Omenetto, N., 2004. Comparing several atomic spectrometric methods to the super stars: special emphasis on laser induced breakdown spectrometry, LIBS, a future super star. *Journal of Analytical Atomic Spectrometry* 19:1061-1083.

Yalcin, S., Crosley, D.R., Smith, G.P., Faris, G.W., 1999. Influence of ambient conditions on the laser air spark. *Applied Phys*ics 68:121-130.